



TAMPEREEN TEKNILLINEN YLIOPISTO
TAMPERE UNIVERSITY OF TECHNOLOGY

Julkaisu 798 • Publication 798

Kimmo Kaunisto

**Energy and Electron Transfer in Organic Multilayered
Thin Films Containing Oriented Porphyrin–Fullerene Dyad**



Tampereen teknillinen yliopisto. Julkaisu 798
Tampere University of Technology. Publication 798

Kimmo Kaunisto

Energy and Electron Transfer in Organic Multilayered Thin Films Containing Oriented Porphyrin–Fullerene Dyad

Thesis for the degree of Doctor of Technology to be presented with due permission for public examination and criticism in Festia Building, Auditorium Pieni Sali 1, at Tampere University of Technology, on the 27th of March 2009, at 12 noon.

Tampereen teknillinen yliopisto - Tampere University of Technology
Tampere 2009

ISBN 978-952-15-2128-7 (printed)
ISBN 978-952-15-2154-6 (PDF)
ISSN 1459-2045

Abstract

Photoinduced intermolecular energy and electron transfers in organic multilayered thin films were studied using electrical and spectroscopic methods. Intra- and interlayer processes were mainly investigated by the time-resolved Maxwell displacement charge and flash-photolysis techniques. Electrochemical photocurrent measurements were used to characterize the photovoltaic properties of the model thin film photocells. The samples were prepared by the Langmuir–Blodgett and spin-coating methods as ordered film structures to provide a parallel vertical electron transfer in all parts of the films. To demonstrate the role of each functional layer in photoinduced reactions, various layer sequences were analyzed and the results from different measurement methods were combined to identify the processes in the films.

A monolayer of oriented porphyrin–fullerene dyad, an electron donor–acceptor molecule, was used to initiate the vectorial electron transfer in the films. A phenyl vinyl thiophene derivative, PVT3, was shown to be capable of both energy and secondary electron transfers to the porphyrin–fullerene dyad when deposited adjacent to the porphyrin moiety. The charge separation distance was extended and charge separated state lifetime was prolonged by depositing poly(hexylthiophene), PHT, in contact with PVT3. In the final charge separated state of such a complex film, the holes are located in the PHT network and the electrons in the fullerene sublayer with the charge recombination in a time domain of seconds. Poly(phenylene quinoxaline), PPQ, was used as an electron acceptor from the fullerene radical anion, increasing the charge separation lifetime for a porphyrin–fullerene–PPQ layer sequence.

Crucial role of the excited porphyrin–fullerene dyad for the overall charge transfer efficiency in the cells with a phthalocyanine derivative, ZnPH4, as an electron donating moiety to the dyad, was demonstrated. The electron transfer from ZnPH4 to the porphyrin cation was shown to be extremely efficient yielding the phthalocyanine cation and fullerene anion moieties. In addition, the electron transfer from PHT to ZnPH4 was demonstrated to be efficient in the corresponding heterojunction.

An electrical signal lifetime was longer compared to that of the optical signal, although the same final transient charge separated state of the film was monitored. The difference in decay times is explained by charge ejection to the molecular environment as the final charge separated state of the system, generating the long-lived free charges that affect more the electrical signal but are less pronounced in the optical signal.

Preface

First of all I wish to thank my supervisor, Professor Helge Lemmetyinen for giving me the possibility to join his group, and finish the Thesis on the fascinating field of photochemistry. I also thank him for the excellent research facilities. Professor Nikolai Tkachenko I thank for all his help during the work.

I want to express my gratitude to Dr. Vladimir Chukharev. Vova's persistent help both in the practical and theoretical issues was indispensable for finalizing my Thesis. Dr. Alexander Efimov I wish to thank for the successful compounds. I am grateful to Dr. Tommi Vuorinen for all his help throughout the work but especially for his expertise at the early stages of my research. I also want to express my appreciation to all the other co-authors of the publications.

For the pleasant work atmosphere I am grateful to all the colleagues in the chemistry laboratory. Especially I want to mention Dr. Riikka Lahtinen. My long term co-workers Dr. Marja Niemi and Anne Kotiaho I wish to thank for sharing this time and science with me.

Finally, I thank my loving parents, Salme and Reino for all the encouragement during the life and for letting me always to make my own decisions, while greatly supporting me in all the turns. Most of all I want to thank my fiancée Sanna for being on my side.

This work was carried out at the Department of Chemistry and Bioengineering (former Institute of Materials Chemistry), Tampere University of Technology in years 2005–2008. The Finnish National Graduate School of Nanoscience and the Organic Solar Cell project of the TEKES Nanotechnology Programme are gratefully acknowledged for funding.

Tampere, March 2009

Kimmo Kaunisto

List of publications

The Thesis is based on the work contained in the following publications, which will hereafter be referred by their Roman numerals:

I Photoinduced electron transfer and photocurrent in multicomponent organic molecular films containing oriented porphyrin–fullerene dyad

Kimmo Kaunisto, Tommi Vuorinen, Heidi Vahasalo, Vladimir Chukharev, Nikolai V. Tkachenko, Alexander Efimov, Antti Tolkki, Heli Lehtivuori, and Helge Lemmetyinen

J. Phys. Chem. C **2008**, *112*, 10256–10265.

II Long-lived charge separated state in molecular films containing porphyrin–fullerene dyad

Kimmo Kaunisto, Vladimir Chukharev, Nikolai V. Tkachenko, and Helge Lemmetyinen

Chem. Phys. Lett. **2008**, *460*, 241–244.

III Photoinduced charge transfer through films containing poly(hexylthiophene), phthalocyanine, and porphyrin–fullerene layers

Kimmo Kaunisto, Heidi Vahasalo, Vladimir Chukharev, Nikolai V. Tkachenko, Paola Vivo, Marja Niemi, Antti Tolkki, Alexander Efimov, and Helge Lemmetyinen

Thin Solid Films **2009**, *517*, 2988–2993.

IV Energy and electron transfer in multilayer films containing porphyrin–fullerene dyad

Kimmo Kaunisto, Vladimir Chukharev, Nikolai V. Tkachenko, Alexander Efimov, and Helge Lemmetyinen

J. Phys. Chem. C **2009**, *113*, 3819–3825.

The following publications, where the contribution from the author has been minor, are related to the Thesis:

V Photoinduced electron transfer in Langmuir–Blodgett monolayers of porphyrin–fullerene dyads

Tommi Vuorinen, Kimmo Kaunisto, Nikolai V. Tkachenko, Alexander Efimov, Helge Lemmetyinen, Alexander S. Alekseev, Kohei Hosomizu, and Hiroshi Imahori
Langmuir **2005**, *21*, 5383–5390.

VI Photoinduced electron transfer in multilayer self-assembled structures of porphyrins and porphyrin–fullerene dyads on ITO

Marja Isosomppi, Nikolai V. Tkachenko, Alexander Efimov, Kimmo Kaunisto, Kohei Hosomizu, Hiroshi Imahori, and Helge Lemmetyinen
J. Mater. Chem. **2005**, *15*, 4546–4554.

VII Photoinduced interlayer electron transfer in alternating porphyrin–fullerene dyad and regioregular poly(3-hexylthiophene) Langmuir–Blodgett films

Tommi Vuorinen, Kimmo Kaunisto, Nikolai V. Tkachenko, Alexander Efimov, and Helge Lemmetyinen
J. Photochem. Photobiol., A **2006**, *178*, 185–191.

VIII Kinetics of photoinduced electron transfer in polythiophene–porphyrin–fullerene molecular films

Tommi Vuorinen, Kimmo Kaunisto, Vladimir Chukharev, Nikolai V. Tkachenko, Alexandre Efimov, and Helge Lemmetyinen
J. Phys. Chem. B **2006**, *110*, 19515–19520.

Table of contents

Abstract.....	i
Preface	ii
List of publications	iii
Table of contents	v
Abbreviations and symbols.....	vii
1. Introduction	1
2. Background	3
2.1. Photovoltaic principles.....	3
2.1.1. Inorganic solar cells.....	3
2.1.2. Third generation solar cells.....	4
2.2. Donor–acceptor assembly	7
2.2.1. Porphyrin and phthalocyanine.....	8
2.2.2. Fullerene	9
2.2.3. Porphyrin–fullerene dyad.....	10
2.3. Conducting polymers	10
2.4. Langmuir–Blodgett films	13
2.5. Aim of the study	15
3. Materials and methods.....	16
3.1. Compounds.....	16
3.2. Spectroscopic methods.....	18
3.2.1. Steady-state absorption and fluorescence	18
3.2.2. Time-resolved absorption and fluorescence	18
3.3. Electrical methods.....	20
3.3.1. Photovoltage.....	20
3.3.2. Photocurrent	22
4. Results and discussion	23
4.1. Film deposition	23
4.1.1. Langmuir–Blodgett films.....	23
4.1.2. Spin-coated films.....	26
4.1.3. Layer arrangement in model cells	27
4.2. Energy transfer.....	29

4.3. Electron transfer.....	31
4.3.1. PVT3 as electron donor to porphyrin–fullerene dyad	31
4.3.2. PHT as electron donor	34
4.3.3. PPQ as electron acceptor from fullerene	35
4.3.4. ZnPH4 as electron donor to porphyrin–fullerene dyad	36
4.4. Photocurrent	39
4.4.1. Step-wise photocurrent	39
4.4.2. Action spectra and current–voltage curves	42
4.5. Electrical and optical signal decays	43
4.6. Organic photovoltaic cell design	44
4.7. Future perspectives	46
5. Conclusions	47
References	48

Abbreviations and symbols

A, A	acceptor, absorbance, area, PPQ
ΔA	absorption change
AFM	atomic force microscopy
a_i	pre-exponential factor
C_s	capacitance of a thin film sample
C_{60}	buckminsterfullerene
CR	charge recombination
CS	charge separation/separated
CT	charge transfer
D	donor, PHT
D–A	electron donor–acceptor
DHD6ee	61,62-diethyl [10,20-(3-(2-hydroxyethoxy)-phenyl)porphyrin-5,15-diylbis(1-phenyl-3-oxy)diethylene] 1,9:49,59-bismethano[60]fullerene-61,61,62,62-tetracarboxylate
E	ZnPH4
ENT	energy transfer
ET	electron transfer
F	fullerene C_{60}
HOMO	highest occupied molecular orbital
$h\nu$	energy of a photon
I_{pc}	photocurrent with zero bias voltage
IPCE	incident photon-to-current efficiency
IR	infrared
ITO	indium-tin-oxide
IV	current–voltage
L	PVT3
LB	Langmuir–Blodgett
LS	Langmuir–Schaeffer
LUMO	lowest unoccupied molecular orbital
mma	mean molecular area
MV^{2+}	methyl viologen

ODA	<i>n</i> -octadecylamine
P	porphyrin
P-F	porphyrin–fullerene (C ₆₀) dyad
PC	photocurrent
PHT	poly(3-hexylthiophene-2,5-diyl)
PMT	photomultiplier
PPQ	poly(<i>p</i> -phenylene-2,3'-bis(3,2'-diphenyl)-quinoxaline-7-7'-diyl)
PV	photovoltage
PVT3	1- <i>tert</i> -butyl-3,5-bis-[(E)-2-[2,2':5',2'']terthiophene-5-yl-vinyl]-benzene
R_{in}	amplifier input resistance of the TRMDC measurement circuit
S_0	ground state
S_1	the first electronic excited singlet state, Q band
S_2	the second electronic excited singlet state, Soret band
TBD6a	61,62-[10,20-(3,5-di- <i>tert</i> -butylphenyl)porphyrin-5,15-diylbis(1-phenyl-3-oxy)di-ethylene] 1,9:49,59-bismethano[60]fullerene-61,61,62,62-tetracarboxylate
TCSPC	time-correlated single photon counting
TRMDC	time-resolved Maxwell displacement charge
U_{out}	photovoltage amplitude
UV	ultraviolet
Vis	visible light
ZnDHD6ee	61,62-diethyl [10,20-(3-(2-hydroxyethoxy)-phenyl)porphyrin-5,15-diylbis(1-phenyl-3-oxy)diethylene zinc (II)] 1,9:49,59-bismethano[60]fullerene-61,61,62,62-tetracarboxylate
ZnPH4	zinc 1(4),8(11),15(18),22(25)-tetrakis[3-(hydroxymethyl)phenoxy]phthalocyanine
Å	angstrom, 10 ⁻¹⁰ m
ϵ	molar absorption coefficient
λ_{ex}	excitation wavelength
τ_i	fluorescence lifetime
$\tau_{1/2}$	half-life
Π	surface pressure

1. Introduction

Most of the mankind's energy need is covered with the non-renewable energy sources such as oil, coal, and natural gas [1]. Combustion of these fossil fuels has harmful effects on Earth's ecosystem by exposing air and water systems to pollutants like nitrogen oxides, sulfur dioxide, and heavy metals. Carbon dioxide, as the main combustion product of the fossil fuels, is considered to be one the most prominent contributors to the greenhouse effect accelerating global warming [2].

The limited supply of non-renewable energy sources has created, together with their harmful side-effects, demand for sustainable and clean energy sources such as solar, hydroelectric, and wind power. Energy emitted by the sun onto the Earth (120 000 TW [3]) exceeds 8000 times the annual energy need of the humankind (15 TW [1]), and therefore makes the sun as the ultimate energy source. Therefore, circa 0.02 % solar energy harvesting efficiency would be enough to replace all the other energy sources by the photovoltaic technology. The energy produced [3] by the photovoltaic and solar thermal panels is only about 1 and 15 GW, respectively, showing the need to overcome cost-efficiency limiting factors in solar energy utilization.

Since the introduction of the first solar cell in 1941 [4,5], photovoltaic technology has evolved but still to date most of the photovoltaic devices are based on the semiconductor *p-n* junction [6,7]. Together with the conventional semiconductor based photovoltaic, more cost-effective dye-sensitized and organic solar cells have been introduced [7–16]. Light-to-current efficiency and overall performance of these third generation photovoltaic have enhanced steadily [10,17–21], and dye-sensitized photocells are already commercially available [10].

Systems designed to achieve the light energy to electric current conversion are based on photoinduced charge carrier generation, which is in organic photovoltaic typically produced by a photoinduced electron transfer (ET) reaction between donor and acceptor sites. In the natural photosynthetic reaction center, the photoinduced ET is used to ignite the reaction chain leading to the conversion of light energy and carbon dioxide to sugars and oxygen [22,23]. The working principle of this Earth's most crucial reaction pathway is mimicked in artificial photovoltaic systems with much simpler molecular architecture. In the natural photosynthesis, chlorophylls are utilized to harvest energy of photons and transfer it to the reaction center [23]. In artificial systems, chlorophylls are typically replaced with similar

macrocyclic compounds, such as porphyrins or phthalocyanines, as light absorbers at the visible region and as electron donating assemblies [24–26].

Electron donating and accepting parts, with typically at least one of them being capable of absorbing light energy, are needed to enable the photoinduced ET reaction. Close contact of the chromophores is required for an efficient charge separation (CS) [27,28] but as a drawback, in such systems charge recombination (CR) is fast as well. Slowing down the CR is desired in order to utilize the potential of the charge separated (CS) state in the following processes [29]. Fullerene has gained a lot of interest as an electron accepting moiety [30–32] because of its excellent electron pooling properties [31,33] and rather slow back ET rate [34]. The CR can be retarded even more by evacuating charges further apart with secondary electron donors and acceptors [VII,29,35]. Photophysical interaction between the chromophores must be analyzed in detail to construct molecular assemblies with desired charge transfer (CT) characteristic.

In the present work, photoinduced intermolecular energy and electron transfer reactions were studied in sandwich-like organic multilayer film structures using electrical and spectroscopic methods. The primary ET from porphyrin to fullerene in a covalently linked electron donor–acceptor (D–A) dyad [II,V,27] was used to initiate the electron movement in perpendicular to the plane of the films. A thiophene derivative was utilized as an energy and electron donor to the dyad. A phthalocyanine derivative and a *p*-type semiconducting polymer were used as hole conducting moieties (electron donors) in the molecular systems. An *n*-type semiconducting polymer was studied as an electron acceptor from the fullerene radical anion.

The compounds and the constructed film structures were studied as possible candidates for organic photoactive thin film devices such as solar cells.

2. Background

A brief introduction to the photovoltaic principles and the molecular assemblies capable of the photoinduced ET is given in this chapter. A short introduction to the conducting polymers and the Langmuir–Blodgett film deposition theory is provided as well.

2.1. Photovoltaic principles

The photovoltaic effect used in solar cells enables direct conversion of light energy emitted by the Sun into electricity.

Possibility of obtaining photovoltaic applications with intriguing advantages such as flexibility, thinness, lightweight, and low cost make organic electronic materials attractive candidates for solar cells [19,36–39]. Power conversion efficiency of an organic photocell has increased steadily [14,15,18,19,21] and model devices with efficiency exceeding 6 % [17,40] have been introduced, being, however, far from the efficiencies of their inorganic counterparts (typically in the range of 10–15 %) to date [6]. High production costs of the conventional solar cells have limited their large-scale utilization for electricity production [6].

Photovoltaic applications capable of the light energy to electric current conversion can be divided to the first, second, and third generation devices by their physics. The first generation devices [7,41] are based on silicon wafers being the most used solar cells in the markets to date [20]. The second generation [6,8] is based on thin film technology of inorganic semiconductors, i.e. basically a thin film approach of the first generation concept. The third generation consists organic [20,42–45] and organic-inorganic composite [11,46–50] devices. Long-term future of photovoltaic will be based on second and third generation devices since the first generation cells are unlikely to become any more cost-efficient [6,8,44].

2.1.1. Inorganic solar cells

A conventional photovoltaic cell is constructed by forming a p - n junction between p -doped (electron deficit) and n -doped (excess of electrons) inorganic semiconductor (typically silicon) [7]. The work function difference between the p - and n -type parts results a transition region with a built-in electric field at the interface. After the light absorption, the excited

electrons in the conduction band and the corresponding holes in the valence band (throughout the *p-n* junction volume) are separated by selective contacts of the *n*- and *p*-type regions with the conduction and valence bands, respectively [7]. The charge extraction is reliant on the built-in electric field to enhance the conversion process. The generated negative and positive charge carriers are collected to the electric circuit via the corresponding electrodes. Rather good electrical conductivities of doped semiconductors enable efficient charge ejection to the external circuit.

In the second generation photovoltaic, a thin layer of photoactive material is deposited on a supporting substrate keeping, however, the basic operation principle same as in the conventional silicon wafer based cells [6,51,52]. Thickness of the semiconducting material can be as low as 1 μm , and thus almost any material is inexpensive enough to be used in the cells. Hydrogenated alloy of amorphous silicon and cadmium telluride have been among the most successful materials for such devices reaching power conversion efficiencies typically from 9 to 12 % [52]. The thin film technology reduces substantially the material consumption improving the cost-efficiency and giving the highest power-to-weight ratio of any photovoltaic to date. To further improve the photovoltaic performance of the thin film concept, multi-junction devices (tandem cells) with efficiencies above 30 % have been introduced [51].

2.1.2. Third generation solar cells

The distinguished characteristic of organic solar cells in contrast to the conventional ones is the mechanism of charge carrier generation [44]. In organic solar cells the charge carriers are generated and simultaneously separated across the heterointerface in contrast to the free electron–hole pairs that are directly produced in the bulk inorganic semiconductors and are separated at the junction as a subsequent process. Photoexcitation (bound electron–hole pair, exciton) in organic cells is transiently localized and cannot thermally dissociate. Charge generation via interfacial exciton dissociation results in a photoconversion process that differs from that in conventional devices.

Organic electronic materials exhibit poor charge carrier mobility and small exciton diffusion length compared to the inorganic semiconductors [43]. However, the poor charge mobility is partly balanced with high absorption coefficients (typically $> 10^5 \text{ cm}^{-1}$) of organic compounds, giving relatively high absorption for layers even $< 100 \text{ nm}$ thick.

The first organic solar cells were based on a single organic layer between two metal electrodes of different work functions [42,43,53]. The rectifying behavior of such a device can be explained by formation of a Schottky barrier between the metal of lower work function and a *p*-type organic layer. This provides a depletion region with strong electric field in which exciton dissociation to charge carriers takes place. Due to the small exciton diffusion length of most organic materials (< 20 nm), only minor fraction of the generated excitons contribute to the photocurrent (PC). Such a device is exciton diffusion limited since an increase in the film thickness (i.e. in the sample absorbance) does not enhance the charge extraction because excitons further away from the depletion region are unable to dissociate as free charges. For such photocells low power conversion efficiencies, typically in the range of 10^{-3} to 10^{-2} %, are obtained [43].

The most developed organic photovoltaic to date are based on an electron D–A heterojunction concept (D–A photocells) creating a large potential drop between the donor and acceptor sites [15,16,19,38,42,43,45]. The exciton dissociation into the free charge carriers is mediated by this strong interfacial electric field caused by the abrupt change of potential energies at the interface. The photoinduced CS takes place when an exciton reaches such an interface within its lifetime. The efficiency of charge carrier generation in organic solar cells is still far from those 80–90 % values typical in conventional devices. The D–A assembly is sandwiched between the electrodes matching the acceptor LUMO (lowest unoccupied molecular orbital) and donor HOMO (highest occupied molecular orbital) levels with the cathode and anode work functions, respectively, for efficient charge collection at both electrodes.

To reach the electrodes, the charge carriers need a driving force that typically results from the gradient in the electrochemical potentials of electrons and holes in the D–A junction [42,43]. The gradient is established by the difference between the donor HOMO and acceptor LUMO levels creating the field induced drift current. The release in electron energy is used to separate electron and hole from their Coulomb potential. The second driving force is the concentration gradient of the respective charges producing the diffusion current. Charge transport after the exciton dissociation proceeds by hopping between localized states rather than transport within a band (as with inorganic semiconductors) resulting low mobilities and decreased charge collection at the electrodes compared to conventional semiconductor cells [15]. The CR in D–A photocells is greatly reduced compared to the single layer concept since electrons and holes travel in distinct *n*- and *p*-type materials, respectively, and thus are separated from each other.

Light energy conversion to electric current in organic photovoltaic can be divided into four steps: (i) exciton formation as a result of photon absorption, (ii) exciton diffusion to the D–A interface, (iii) exciton dissociation into the separated charge carriers, (iv) charge transport to the corresponding electrodes (electrons to the cathode and holes to the anode).

To construct the electron D–A interface, either a bilayer or bulk heterojunction [54] concept can be utilized [15,42,43]. In a bilayer device, *p*-type electron donor and *n*-type electron acceptor materials are in separate layers and stacked together with a planar interface between them. The CS takes place at the interface, and therefore a bilayer device is exciton diffusion limited. The efficiency of such a cell is limited by the charge generation in the region < 20 nm around the interface. Thus, an increase in the film thickness creates only an optical filtering effect decreasing the photovoltaic response of the device. Power conversion efficiencies of circa 4 % have been reported for the bilayer device architecture [55,56].

In a bulk heterojunction device, donor and acceptor materials are blended together in a bulk volume to form such an interpenetrating network in which the D–A interface is within the exciton diffusion length from the absorbing site [42,43]. The major advantage of the bulk heterojunction is a large interfacial area between the donor and acceptor parts that enables efficient exciton dissociation within their lifetime in the whole film volume. However, since the donors and the acceptors are mixed together as a homogenous blend, there is no preferred net direction in which the charge carriers should move after the exciton dissociation. Therefore, a symmetry breaking condition (e.g. selective electrodes with different work functions) is needed to generate a driving force to enhance the charge collection at the electrodes. Otherwise, only concentration gradient acts as a driving force for charges. In addition, continuous pathways for the *p*- and *n*-type networks to the contacts must be established making the bulk heterojunction devices extremely sensitive to the nanoscale morphology of the blend. Efficiencies of circa 3.5 % have been reported for the bulk heterojunction concept [57,58].

The third generation photocells are majority carrier devices where the carrier generation, separation, and recombination takes place at the interface, in contrast to the inorganic counterparts that are minority carrier devices in which these processes happen in the bulk semiconductor [44]. Despite the intensive research in the field of organic photovoltaic, the fundamental physics of organic D–A photocells is still poorly understood [15].

One the most advanced organic-inorganic composition device is a dye-sensitized solar cell, also known as the Grätzel cell [7,11,49,59–61]. The dye-sensitized photocell is composed of an organic dye as the light absorber, a nanocrystalline metal oxide (typically

titania, TiO₂) as an electron transporting moiety, and a liquid (or a solid) hole transporting material. The TiO₂ *n*-type semiconductor is used to capture a high energy photoexcited electron from the dye molecule and transport it to the electrode via its conduction band. The remaining positive hole on the valence band of the dye is replenished by an electron from the hole transporting medium. Power conversion efficiency of circa 11 % has been reached for the dye-sensitized cell with solution based electrolyte [11].

In addition, to construct an efficient inorganic-organic hybrid solar cell, semiconducting nanocrystals (e.g. CdSe, ZnO, or PbS) can be blended together with semiconducting polymers as in the bulk heterojunction concept [46,47,50,62]. Excitons are dissociated with high yield as free charge carriers at the inorganic-organic interface. Efficiency of about 3 % has been reported for such a cell [63].

2.2. Donor–acceptor assembly

The photoinduced ET between distinct molecular sites is reminiscent of the reaction center in the natural photosynthesis system. During the process, an electron is transferred from a donor (D) to an acceptor (A) resulting in oxidized and reduced species, respectively. Close center-to-center distance between the donor and acceptor sites, as well as light absorbing ability of at least one of the chromophores involved is required for the photoinduced ET to take place. If the donor and the acceptor are parts of the same molecule, the ET is called intramolecular, and intermolecular if they are not. The photoinduced ET in a covalently linked D–A dyad molecule, with the donor site being capable of absorbing light, can be presented as follows:



where D* is the photoexcited donor, D⁺ is the donor radical cation, A⁻ is the acceptor radical anion, and *hν* represents a photon. In this simple reaction, light energy absorbed by the donor is transformed to the electrochemical potential of the CS state. The HOMO and LUMO energies of the donor need to be higher than the respective energies of the acceptor for the energetically favorable ET in a D–A interface.

If the excited state energies of donor and acceptor are close to each other, energy transfer (ENT) between the sites may take place prior to the ET reaction. This can be presented similarly to the earlier scheme as:



where A^* represents the excited acceptor. In addition, decay back to the ground state may take place from any state without the electron or energy transfer reactions to happen.

Detailed theoretical background for the light-induced and dark ET reactions is given in the classical Marcus theory of electron transfer [64,65].

2.2.1. Porphyrin and phthalocyanine

Porphyrins and phthalocyanines having planar macrocyclic structures are together called porphyrinoids. The parent porphyrin contains four pyrrole subunits connected via methane bridges, and is referred to as porphine (Figure 2.1). Substituted porphines are called porphyrins. Porphyrins have highly π -conjugated macrocyclic structure (22 π -electrons) producing their strong light absorbing character in the visible region and good electron donating properties [25,42,43,66].

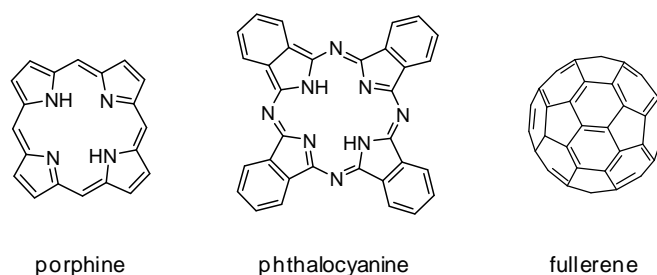


Figure 2.1. Chemical structures of porphine, phthalocyanine, and C_{60} fullerene.

In phthalocyanines, four pyrrole rings are benzo fused to isoindoles and interconnected via aza bridges as shown in Figure 2.1. Phthalocyanines have alternating nitrogen-carbon atom ring structure with four isoindole groups providing the delocalized π -electron system (18 π -electrons), and thus their aromatic nature with similar absorption and ET characteristic to porphyrins [42,43,67]. The photophysical and reduction-oxidation (redox) properties of the macrocycles are, however, different despite the structural similarities [66].

Porphyrins exhibit a strong absorption band, called the Soret band, at circa 410–450 nm (molar absorption coefficient $\epsilon > 200\,000\text{ M}^{-1}\text{cm}^{-1}$ [66]), and four weaker absorption bands, called the Q bands, at wavelengths circa 450–750 nm. The Soret band corresponds to the transition from the ground state (S_0) to the second electronic excited singlet state (S_2) and the Q band transitions from the S_0 to the first excited singlet state (S_1). The phthalocyanines

possess the corresponding Soret and Q band absorptions at wavelengths circa 320–360 and 670–750 nm, respectively. Compared to porphyrins, phthalocyanines exhibit much stronger absorbance at the Q band region ($\epsilon \approx 200\,000\text{ M}^{-1}\text{cm}^{-1}$ [25]) making them better candidates for light energy harvesting materials.

Properties of the porphyrenoids, e.g. redox potentials and solubility, can be altered by peripheral substituents or introducing desired metal atom into the central cavity of the macrocycle [68]. Non-metallated porphyrins and phthalocyanines with two imine hydrogens in the central cavity are called free-base structures.

Porphyrins have important roles in some biological processes [66,69], as well as in artificial energy and electron transfer systems [22,70–73]. Phthalocyanines are traditional industrial dyes, but have been utilized e.g. as optical recording materials [74], catalysts for oxidative degradation of pollutants [75], photosensitizers in photodynamic therapy [76], and in energy and electron transfer systems [24,70,77].

2.2.2. Fullerene

The general class of carbon compounds with close cage structure is called fullerenes. Number of carbon atoms in fullerenes range from 20 to 100 [78,79], while the most common and the smallest stable one is a buckminsterfullerene, C_{60} , with 60 carbon atoms [80–82]. C_{60} has highly symmetric truncated icosahedron structure with 12 pentagonal and 20 hexagonal faces resembling the shape of football (Figure 2.1) with diameter of circa 0.7 nm [82]. Carbon atoms are sp^2 -hybridized in a C_{60} molecule providing the sea of 60 delocalized π -electrons over the molecule surface and the aromatic nature of buckminsterfullerene [80–82].

C_{60} is capable of reversibly accepting six additional electrons [33,83] making it a good electron acceptor, and thus many fullerene based electron D–A assemblies have been introduced [84–87]. The rigid spherical carbon framework of C_{60} is stable, but not totally nonreactive and therefore it can be functionalized [80,88]. Functionalization does not change the properties of fullerene, although it disturbs the delocalization of the π -electron system [34]. C_{60} possesses a moderate absorbance throughout the visible region and more intense absorption in the UV region shorter than 300 nm.

In the Thesis, fullerene refers to C_{60} that was used as a primary electron acceptor in most of the studied CT systems.

2.2.3. Porphyrin–fullerene dyad

In a porphyrin–fullerene dyad, electron donating (porphyrin) and accepting (fullerene) sites are covalently linked to each other. Such dyads have been proved to be capable of the photoinduced intramolecular ET from porphyrin to fullerene yielding the porphyrin cation and fullerene anion moieties [VI,24,26,31,32,72,73,89–96]. Because of stronger light harvesting ability of porphyrin in the visible region, mainly the porphyrin part is photoexcited and fullerene acts as an electron acceptor in its ground state.

In the dyads, the ENT from porphyrin to fullerene competes with the ET due to the almost equal excited state energies of the compounds [27,97], and may be faster in nonpolar solvents than the ET [32,98,99]. The complete CS state in the porphyrin–fullerene dyads is demonstrated to be formed via the intramolecular exciplex state [27,95], which is related to the closeness of the excited state energies of the donor and acceptor moieties.

Short center-to-center distance in covalently linked D–A dyads provides the fast CS, but as a drawback, also the back ET is often rapid. By expanding the linker length [100] or introducing secondary electron donors or acceptors [VII,29,99,101–103] to the system, longer charge separation distance is reached prolonging the lifetime of the CS state. However, the longer distance between the donor and acceptor sites decreases the CS yield by reducing the overlap between the molecular orbitals of donor and acceptor parts. Using two molecular linkers to attach the donor and acceptor parts to each other, more pronounced face-to-face orientation between the sites is achieved increasing the CS efficiency [23,27].

2.3. Conducting polymers

Conducting polymers were discovered in 1976 [104,105]. The discovery of oxidative doping of polyacetylene, to modify its conductivity over eleven orders of magnitude from insulator to metallic, initiated an extensive research and development on the field of organic semiconductors.

Unique features of organic materials with electrical properties of metals are responsible for growing interest in the development of conducting polymers [106–109]. The major advantages of conducting polymers are their attractive mechanical properties and processibility combined with the electrical and optical characteristics of metals and inorganic semiconductors. Polymers have ability to coat large areas providing applications e.g. for displays [110] and mechanically flexible electronics [111]. Conducting polymers have been

utilized in thin film electronics such as thin film transistors [112], memory elements [113], light emitting diodes [111,114], polymer photodetectors [115], and photovoltaic cells [116].

All the valence electrons of traditional polymers are bound in sp^3 -hybridized covalent bonds, and thus there are no mobile electrons in their backbone for electronic transport yielding the insulator characteristic of these materials. Intrinsic electrical conductivity of polymers arises from the conjugated π -electron system of the polymer backbone formed in the sp^2 -hybridization of carbon 2s and 2p orbitals [42,43,106,108,109,117,118].

The free p-orbitals of the sp^2 -hybridized successive carbon atoms along the linear carbon chain overlap to produce the π -electron delocalization over the polymer, and therefore creating a highway for charge mobility along the polymer backbone. The π -band is divided into π -bonding (valence band) and π^* -antibonding (conduction band) molecular orbitals. Since each orbital can hold two electrons per atom, the π -band is completely filled and the π^* -band remains empty. Because there is the lack of partially filled bands and a rather small energy gap between the π -orbitals (circa 1–3 eV), conjugated polymers exhibit semiconductor characteristic and possess absorption in the visible region. Pristine (undoped) polymers with intrinsic conductivity are typically composed of carbon, hydrogen, and simple heteroatoms such as nitrogen or sulfur [117]. Conjugated polymers to date are in their pristine form insulators or exhibit only semiconducting properties [108].

Conductivity of the conjugated polymers can be controlled over the range from insulator to metallic by doping [108,109,117]. In doping, electrochemical potential (the Fermi level) of polymer is moved into the energy region with high density of electronic states. Doping introduces into the polymer charge carriers that are able to move along the π -bonded highway of polymer backbone. Charge carrier in a repeating unit experiences attraction from the neighboring one resulting delocalization of carriers throughout the polymer chain, and thus giving origin to the charge mobility. Mobility of charges is extended over the bulk through the interchain ET.

In the chemical doping, chemical dopants are used to oxidize (*p*-type conductor) or reduce (*n*-type conductor) the conjugated polymer to create positive or negative charges, respectively, into the polymer chain [108,109,117]. Conjugated polymers can be doped to high density of charge carriers since every repeating unit has potential for a redox reaction. Iodine and bromine are typical oxidants used for the *p*-type doping and alkali metals typical reductants for the *n*-type doping. The *n*-type doping is much less common since elemental oxygen from the atmosphere reacts with the electron rich polymer dedoping the polymer back to the neutral state. Besides the chemical doping, polymers can be doped e.g. by

electrochemical, photodoping, or acid–base protonation processes to create additional charge carriers to the structure [108,109,117].

Electrical conduction in conjugated polymers is a complex phenomenon, and to date no single model can be used to comprehensively describe it [108,117]. Conduction in polymers differs from that in conventional semiconductors and it is often referred to as redox conduction rather than the electronic one [108,109,117]. In polymers, electrical conductivity is ascribed mainly to the motion of charge carriers such as polarons, bipolarons, and solitons. Polaron is a charge stabilized by a local structural distortion in the polymer chain. Bipolaron is combination of two polarons, and is formed with high doping levels where bipolaron is more favourable than two individual polarons. Formation of bipolaron may lead to generation of two distinct degenerate energy levels that is called a soliton. The soliton can be described as domain boundary between the two possible degenerate ground state configurations of the polymer chain. The soliton (two delocalized charges) is formed from a single bipolaron and is able to move along the polymer backbone. Polarons, bipolarons, and solitons are delocalized over several monomer units and electrical conductivity is characterized best as hopping of charges between the delocalized charged states. Delocalized charges form energy bands in bulk decreasing the actual band gap of the polymer, and thus increasing the semiconducting characteristic of the material. Short conjugation length of polymers is one of the key limiting factors of conductivity.

The discovery of photoinduced ET from conducting polymer to fullerene C₆₀ in year 1992 created new potential applications to utilize the conjugated polymers [119,120]. Since then, numerous studies developing organic photovoltaic by using conducting polymers have been carried out [45,121–127]. Conjugated polymers act typically as electron donors in the ET systems since photoexcitation promotes excited electrons to the polymer antibonding π^* -orbital [109]. The ET rate from a poly(*p*-phenylene vinylene) derivative to fullerene is demonstrated to be three orders of magnitude faster than the competing relaxation processes in the polymer [128], and therefore the ET quantum yield approaches unity. The discovery of extremely fast CS in the conducting polymer/C₆₀ blend initiated vigorous development of the polymer photovoltaic. However, to solve the limiting factors in organic photovoltaic efficiency, new materials with advanced optical and electrical characteristics such as light harvesting capability and conductivity are needed.

2.4. Langmuir–Blodgett films

The Langmuir–Blodgett (LB) technique is a well known method for making highly oriented homogenous organic ultrathin films with the thickness of one molecule (a monolayer), and depositing them onto a solid substrate [129,130].

Films with thicknesses of few nanometers have a potential to be useful components in commercial applications such as displays, sensors, and electronic circuits [129–131]. The LB technique enables precise control over the layer thickness and possibility to construct multilayer structures with desired layer sequences on large areas, making it a powerful thin film deposition method.

Irving Langmuir was the first to perform systematic studies on floating monolayers on water subphase in late 1910's and early 1920's [130]. The first formal detailed description of transferring the floating monolayer onto a solid substrate was given by Langmuir's co-worker Katherine Blodgett in 1935 [132]. Therefore, a floating monolayer is called the Langmuir film and a built-up monolayer assembly the Langmuir–Blodgett film.

The “modern” period of the LB technology dates to the early 1970's when Kuhn and co-workers studied monolayer organization [129,133]. This work was the first study towards the functional systems in a molecular scale and coincides with the beginning of microelectronics revolution, which enabled the practical use of the technique.

The LB film preparation is separated to two steps, the homogenous Langmuir film formation over an aqueous subphase and the actual LB film deposition onto a solid substrate (Figure 2.2) [129,130]. Anisotropic interaction between the molecules of interest and the subphase is needed for homogeneous monolayer formation. Molecules having separated hydrophilic and hydrophobic regions possess amphiphilic nature and have no tendency to form a layer more than one molecule thick when extended over the subphase area. Such molecules are anchored to the aqueous subphase from their hydrophilic end (usually via dipole moments or by hydrogen bonding), while the hydrophobic end is pointing towards the air making the molecule insoluble to the subphase. Polymers and molecules with non-amphiphilic structure (insoluble to the subphase) do not form oriented monolayers with long-range order [129,130]. Such layers have typically thicknesses more than one molecule and display more or less amorphous nature. The LB deposition of non-amphiphilic molecules (including polymers) typically requires mixing them into an amphiphilic matrix.

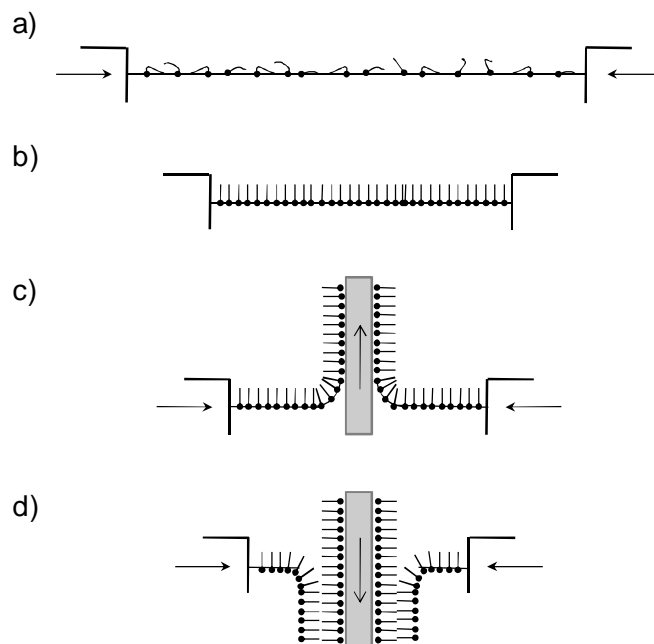


Figure 2.2. The Langmuir–Blodgett method. (a) Amphiphilic molecules extended over the subphase. (b) Formation of the Langmuir film. (c) Langmuir–Blodgett film deposition. (d) Deposition of a multilayer film structure.

The reduction of surface tension by the molecules on it is called the surface pressure (Π) of a monolayer, and it depends on the area available per molecule [129,130]. Reducing the surface area increases the interaction between the molecules, and thus raises the surface pressure. A plot of surface pressure against area per molecule in constant temperature is referred to as a surface pressure–area (Π – A) isotherm. During the monolayer compression the Langmuir film undergoes phase transitions, which are determined by the physical and chemical characteristics of the amphiphile and the subphase. Initially loosely packed and inhomogeneous monolayer, referred to as a two-dimensional gas, over the subphase undergoes transition to a liquid-expanded state if compressed to smaller area. Upon further compression a transition to a liquid-condensed state takes place, and finally a solid state is reached that is followed by the monolayer collapse if further compressed. In the collapse, the oriented homogenous monolayer is destroyed producing a three-dimensional structure.

The monolayer deposition onto a solid substrate is accomplished by moving the vertically oriented substrate through the subphase surface while keeping the surface pressure constant (Figure 2.2c and 2.2d) [129,130]. The floating monolayer is adsorbed onto the substrate, and a multilayer film structure can be deposited by redipping the substrate through the monolayer. The monolayer does not experience any major changes in organization during the deposition [129]. The LB deposition is traditionally carried out in the solid phase

but this is not essential as long as the film is not expanded, i.e. interaction of the molecules in the monolayer is high enough to be deposited unbroken onto a substrate [130]. Typically surface pressures 10–40 mN/m are used for the deposition but to reach the best result, deposition conditions of each compound have to be established empirically. The quality of a deposited LB film is described by a transfer ratio (a ratio between the decrease in the monolayer area during the deposition and the area of the substrate) [129,130]. In the ideal deposition the transfer ratio equals unity. Transfer ratios outside the range of 0.95–1.05 are typically indicative of the poor film homogeneity.

The isotherm can be used to estimate the molecular area of a single molecule. Nevertheless, the measured area per molecule (mean molecular area, *mma*) merely represents an average without a guarantee that it corresponds to the real area of any particular molecule, even in extremely homogenous monolayers [129]. Unrealistically small molecular areas can be obtained as a result of molecule aggregation on the subphase or by formation of a layer thicker than one molecule [129,130]. Various inhomogeneities such as crystalline packing, grain boundaries, and defects (e.g. impurities and holes) typically exist in monolayers even if they were constructed with utmost precaution.

An alternative way for monolayer deposition is to use horizontal dipping instead of the vertical one. In the horizontal method, referred to as the Langmuir–Schaeffer (LS) technique, a horizontally oriented substrate is lowered into contact with the monolayer without penetrating the subphase surface [134]. Similarly to the LB deposition, the monolayer is adsorbed onto the substrate surface.

2.5. Aim of the study

The aim of the Thesis was to study photoinduced energy and electron transfers between organic molecular thin films. The multilayer film concept was introduced to enable multistep ET reactions between the layers. Each layer had its own function in the film system in order to increase the number of CS states and the distance between the positive and negative charges. Increased distance prolongs the lifetime of CS enhancing the probability of charges to be utilized in the following processes. Light harvesting layer was used as an energy transfer assembly to enhance the charge separation.

Photoinduced processes were studied to develop understanding on the interaction between different organic substances in solid state. This knowledge can be utilized in designing organic photovoltaic devices.

3. Materials and methods

This chapter provides a brief introduction to the film characterization techniques used in the Thesis, and describes the studied compounds. More detailed descriptions about the experimental techniques are given in the publications referred by the Roman numerals or references therein.

3.1. Compounds

Molecular structures of covalently linked porphyrin–fullerene dyads DHD6ee [II–IV], TBD6a [I], and ZnDHD6ee [I] used in this study are presented in Figure 3.1. In the DHD6ee and ZnDHD6ee dyads, polar groups are located at the porphyrin end making it hydrophilic, and in TBD6a the polar groups are close to the fullerene moiety. In addition, molecule structures of a phthalocyanine derivative, **ZnPH4** [III,IV], a phenyl vinyl thiophene derivative, **PVT3** [I,IV], a *p*-type semiconducting polymer regioregular poly(hexylthiophene), **PHT** [I–IV], and an *n*-type semiconducting polymer poly(phenylene quinoxaline), **PPQ** [I], used to extend the CS in the studied molecular assemblies are shown in Figure 3.1.

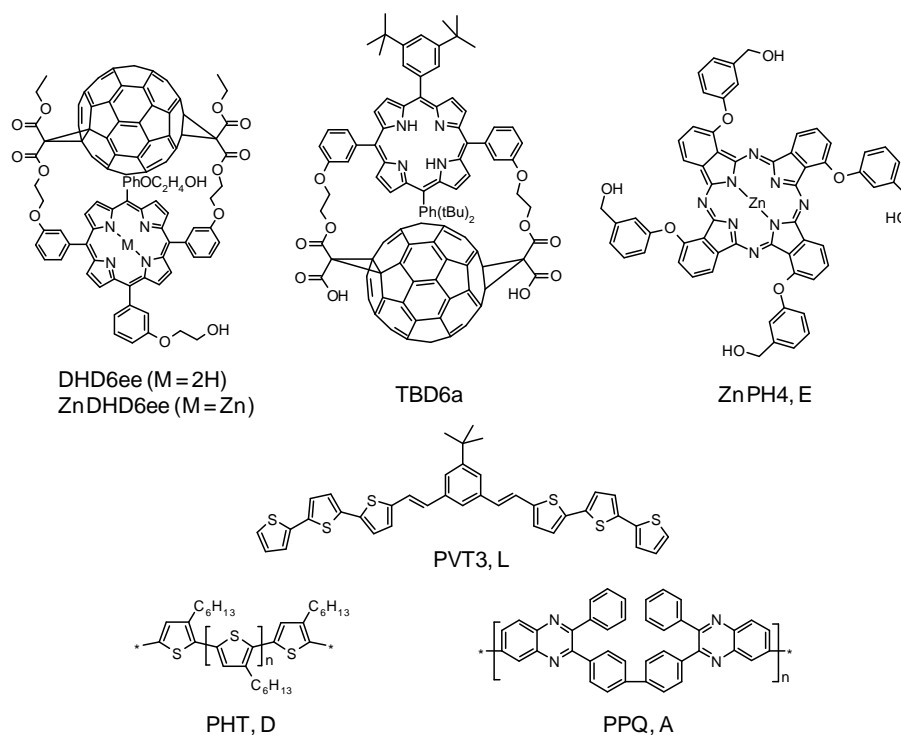


Figure 3.1. Molecule structures and acronyms of the compounds. Porphyrin–fullerene dyads are referred to **P-F** when the film structures are described.

The D–A dyads were utilized to produce the primary photoinduced ET from porphyrin to fullerene initiating the charge transfer to the desired vertical (perpendicular to the plane of the films) direction in the samples. **PVT3** was exploited as light harvesting material in blue region in order to promote energy and electron transfers to a porphyrin–fullerene dyad. **PHT** and **ZnPH4** were used as secondary electron donors and hole conducting materials. Furthermore, **PHT** increased the light harvesting in green region and **ZnPH4** in red region. **PPQ** was studied as an electron acceptor from the fullerene radical anion [135]. The primary ET from porphyrin to fullerene in the D–A dyads [V,27,136], as well as the secondary electron donation from **PHT** to the porphyrin cation of the dyad [VII], have been demonstrated earlier.

In the following, when the film structures are described, the acronym **P-F** is used for simplicity for all the dyads indicating the location of the porphyrin (**P**) and fullerene (**F**) moiety. Compounds **PHT**, **ZnPH4**, **PVT3**, and **PPQ** are denoted as **D** (for electron **D**onor), **E** (for **E**lectron donor), **L** (for **L**ight absorber), and **A** (for electron **A**ceptor), respectively.

The synthesis [137] and the influence of metallization [90] of the dyads are, as well as the synthesis of **ZnPH4** [138], described in the literature. The synthesis of **PVT3** is presented in paper I. Polymer **PHT** was purchased from a commercial source and **PPQ** [135,139] was received from the University of Potsdam. Octadecylamine, ODA, was used as a matrix compound for the LB film preparation.

The studied thin film samples were prepared by the LB [I–IV], LS [I], and spin-coating [III,IV] methods. The LB and LS methods are described in detail in chapter 2.4. The spin-coating is another well-known method to construct uniform thin films on a flat substrate. The studied solution is placed on a substrate, which is then rotated with high speed to spread the fluid over the substrate to form a uniform layer. The film thickness can be altered by varying rotation speed, rotation time, solution concentration, or by changing the solvent. In contrast to the LB method, spin-coated layers are normally thicker than one molecular layer and disordered. Typically, high quality films with thicknesses from few nanometers to micrometer range can be produced by spin-coating.

3.2. Spectroscopic methods

Steady-state spectroscopic techniques were mainly used to determine the deposited film quality and the ground state absorption characteristics of the samples. Time-resolved methods were utilized to identify the photoinduced intra- and interlayer processes in the films by determining the transient states of the chromophores after the photoexcitation.

3.2.1. Steady-state absorption and fluorescence

Absorption spectra of the films were measured with a conventional UV-Vis absorption spectrophotometer in 300–800 nm range. The absorption spectrum provides a way to verify the film transfer in the layer deposition, and was typically used to evaluate the sample quality after each deposition. Furthermore, the absorption spectra were used to determine the wavelength regions where individual chromophores absorb. This was used to select the excitation wavelength in time-resolved measurements so that only a particular chromophore was excited at a time. Time-resolved changes in the absorption after the photoexcitation were interpreted by comparing the ground state spectrum to the time-resolved one [II,IV]. Molecular aggregation can be estimated from the absorption spectra [140,141], and that was utilized to estimate the LB film formation properties of **PVT3** [I]. Absolute absorption values of the samples were used to calculate the photovoltaic parameters of model cells [I,III].

Steady-state fluorescence experiments were performed with continuous excitation and emission intensity was followed in 400–800 nm range. Fluorescence measurements were used to detect the **PVT3** emission quenching due to the photoinduced energy and electron transfer reactions to the **P-F** monolayer [I].

3.2.2. Time-resolved absorption and fluorescence

Optical scheme of the flash-photolysis system used for the time-resolved absorption measurements in micro- to millisecond timescale is shown in Figure 3.2. In the flash-photolysis method, the sample is photoexcited by a strong light pulse called the pump. The pump pulse is used to excite the sample molecules to higher energy levels producing changes in absorption. Reduced population on the ground state produces the decreased ground state absorption (called bleaching) at the corresponding wavelengths. Similarly, transient states formed upon the excitation have their individual absorption characteristics giving rise to the

increased absorption at the respective wavelengths. Thus, due to the population disturbance caused by the photoexcitation, sample undergoes negative and positive absorption changes that are monitored as a function of time at the given wavelengths. Signal decay describes the excited state recombination back to the ground state. Relaxation processes initiated by the pump pulse are monitored by the pulsed or continuous light called the probe, i.e. absorption changes in the probe are monitored as a function of time after the pump excitation.

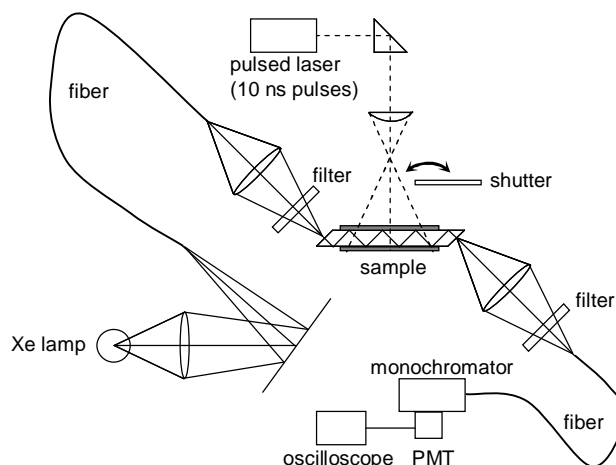


Figure 3.2. Simplified scheme of the flash-photolysis measurement system.

In this study, thin film samples for the laser flash-photolysis experiments were measured by using the total internal reflection mode in order to increase sample absorption [II,IV]. The excitation source was the first ($\lambda_{ex}= 720$ nm) or second ($\lambda_{ex}= 430$ nm) harmonic of a Ti-sapphire laser pumped by the second harmonic of a Q-switched Nd:YAG laser (532 nm), or the third harmonic of the Nd:YAG laser ($\lambda_{ex}= 355$ nm) with 10 ns pulses. Cylindrical lens was used to broaden the excitation pulse to cover the probed part of the sample. Continuous white light from a xenon lamp was used as the probe.

The probe light was focused on 45° end of a substrate using a lens (Figure 3.2). The probe light coming from another end after dozens of internal reflections was collected and transmitted to a monochromator, and finally to a photomultiplier (PMT). A digital oscilloscope was used to record the signal at the given wavelength. Then the wavelength was changed and a new decay curve was measured in the same conditions. This way transient absorption decays were recorded in the absorption range of 450–880 nm in order to obtain time-resolved absorption spectra of the samples. Transient decays at different timescales were measured to compare decay kinetics of the films. Measurements were performed at room temperature in nitrogen atmosphere to inhibit the effect of molecular oxygen.

The time-correlated single photon counting (TCSPC) method was used to determine fluorescence lifetimes of **PVT3** in the films with and without a porphyrin–fullerene dyad monolayer [I]. The fluorescence decays were fitted with a sum of three exponentials. Time resolution of the TCSPC instrument was circa 60–100 ps (full width half maximum of the instrument response function).

3.3. Electrical methods

A photovoltage (PV) method was utilized to study vectorial photoinduced ET in thin film samples. Electrochemical PC experiments were used to study the current generation of model photocells under the illumination. All the electrical measurements were performed in air at room temperature.

3.3.1. Photovoltage

To study photoinduced ET in thin films, the time-resolved Maxwell displacement charge (TRMDC) method [142–144] was used [I,III]. Organized molecular monolayers with similar spatial orientation of the electron donor with respect to the acceptor throughout the whole film can be deposited by the LB method. Similarly, by using the LB and spin-coating methods ordered multilayer film structures with interlayer ET to the same vertical direction in the whole film system can be constructed. The TRMDC method is a powerful tool to measure such a vertical electron movement in perpendicular to the plane of the film.

Simplified scheme of the TRMDC measurement circuit is shown in Figure 3.3. After the photoexcitation, vertical electron movement in the sample induces charges on the electrodes, and the difference of voltage is measured as a function of time. Since the photoactive part of the sample is insulated from the electrodes, the observed TRMDC signal is produced only by the vectorial photoinduced ET in the direction perpendicular to the plane of the film in the active layer. Thus, only the vertical electron movement is detected leaving lateral charge movements unnoticeable. Capacitance of the sample C_s (together with the input capacitance of the amplifier) can be roughly estimated as 200 pF. The sample establishes together with an amplifier input resistance (R_{in}) an RC circuit with a time constant of $\tau_{RC} = R_{in}C_s$. In this study, the used input resistance was 100 M Ω giving the typical time-constant of 20 ms. The TRMDC signals were measured in time domains much shorter than the τ_{RC} resulting to the negligible discharge of the capacitor C_s over the load R_{in} , and therefore the measured voltage

was basically the potential at C_s . Thus, the PV amplitude is directly proportional to the number of CT states and to the distance of CS.

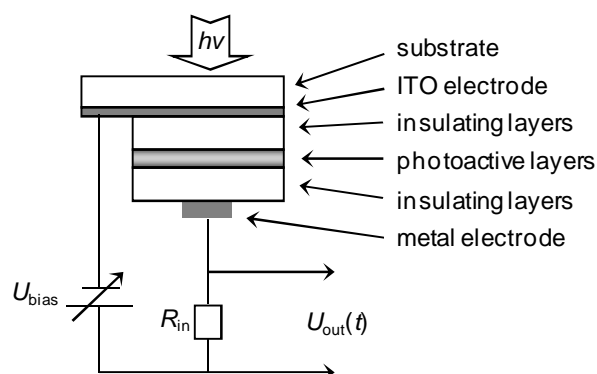


Figure 3.3. Schematic view of the photovoltage measurement circuit.

In this study, samples were excited by 10 ns laser pulses at the wavelengths 430, 436 or 710 nm. The excitation source was a tunable Ti-sapphire laser (pumped by the second harmonic of a Q-switched Nd:YAG laser). The time-profile of the PV decay after the photoexcitation was recorded with a digital oscilloscope. Time resolution of the PV measurements was circa 20 ns determined by the excitation pulse width and the bandwidth of the amplifier. A liquid InGa drop was used as a second electrode. Typically more than ten ODA monolayers were used to insulate the photoactive part from both electrodes.

The PV technique is a direct and simple method to measure ET reactions but it cannot be used to identify the charged species. The method is sensitive to all charges in the sample without assigning them to any specific cation or anion moieties. In addition, studied donor–acceptor sites must have similar spatial orientations for the electronic transitions to be observed, since only vertical charge movement is detected.

The time-resolved spectroscopic [145] methods are typically used to characterize ET reactions. High sample absorbance and excitation power density are often needed for the spectroscopic studies in contrast to the PV experiments. Even a sample with a film thickness of one molecular layer can be measured with the PV technique using rather low excitation intensity. However, the spectroscopic methods usually provide the reaction kinetics revealing also the transient species that are produced in the photoinduced transitions.

3.3.2. Photocurrent

The PC generation characteristics of model photocells were determined by using a three-electrode photoelectrochemical cell [I,III]. In contrast to the PV measurements, the PC response is affected only by the charges that reach the electrodes and are transferred to the electric circuit. Thus, the PC measurements determine the photovoltaic properties of a model photocell, i.e. ability of the cell to generate current under the illumination.

The PC measurements were performed in a three-electrode cell with ITO as a working electrode, platinum wire as a counter electrode, and Ag/AgCl (saturated KCl) as a reference electrode. The ITO electrode was modified by depositing the photoactive films onto it. The counter electrode was in contact with the active layers via the aqueous electrolyte containing 1,1'-dimethyl-4,4'-bipyridinium dichloride (methyl viologen, MV^{2+}) as an electron acceptor. MV^{2+} supports the natural direction of ET in the studied thin film cells. KCl was used as a supporting electrolyte. Model photocells were illuminated step-wise and the current generation was monitored as a function of time. In addition, current–voltage (IV) curves and incident photon to current efficiency (IPCE) spectra were determined. Excitation source was a Xenon lamp coupled with a monochromator and deviations in the excitation intensity were taken into account.

4. Results and discussion

This chapter provides a brief summary about the most significant results introduced in the publications I–IV.

At first, multilayer deposition by the LB and spin-coating methods is introduced. Layer arrangement in the films and the corresponding energy levels of the components are presented to visualize the possible energy and electron transfer scheme in the studied molecular systems. Interaction between the molecular layers after the photoexcitation is identified by analyzing together the results from the different measurement techniques. The photoinduced interaction between **PVT3** and **P-F** was studied, and both the energy and electron transfers were demonstrated to take place. The CT system was further extended by introducing **PHT** to the film structure as an electron donor to **PVT3**. Polymer **PPQ** was utilized as an electron acceptor from the fullerene radical anion. Finally, the phthalocyanine derivative was studied as an antenna layer to **P-F** instead of **PVT3**. A monolayer of oriented porphyrin–fullerene dyad was used to initiate the ET to the desired vertical (perpendicular to the plane of the films) direction in the samples [V]. The PC experiments were used to characterize photovoltaic properties of the model photocells.

For porphyrin and chlorin type of macrocycles, an extremely fast internal conversion $S_2 \rightarrow S_1$ is demonstrated to happen in tens of femtoseconds [27,29,146]. Similar internal conversion is assumed to happen in the phthalocyanine derivative as well. Therefore, intra- and intermolecular ET reactions for such chromophores in excited state are considered to take place from the S_1 state.

4.1. Film deposition

The Langmuir–Blodgett and spin-coating methods were used to construct various film structures to study the photoinduced energy and electron transfers in layered thin films. Absorption spectra of the layered films were sums of their corresponding component spectra indicating successful film deposition and weak ground state interaction between the distinct molecular layers.

4.1.1. Langmuir–Blodgett films

The Π – A isotherms were recorded for the **PVT3** Langmuir films with various concentrations in the ODA matrix, as shown in Figure 4.1, to study the LB film formation

[I]. The LB deposition was not successful for an unmixed **PVT3** layer, whereas mixing the **PVT3** in highly amphiphilic ODA matrix enabled the LB deposition up to 70 mol% **PVT3** layers. The **PVT3** molar fraction was chosen as 70 mol% in further studies as a compromise between the highest surface coverage and the LB film transfer ratio.

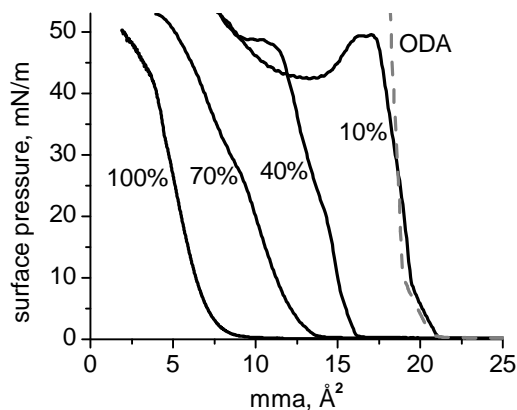


Figure 4.1. Surface pressure–area isotherms for the **PVT3** Langmuir films of molar fractions from 10 to 100 mol% in the ODA matrix, as well as the isotherm for 100 % ODA monolayer.

The mean molecular areas of the mixed films decrease with increasing **PVT3** concentration, nevertheless **PVT3** has larger molecular area than that of ODA ($\sim 18.5 \text{ \AA}^2$ at 30 mN/m). The limiting area of **PVT3** extrapolated from the isotherms is circa 7.5 \AA^2 , while on the basis of molecular structure, values 620 and 80 \AA^2 can be estimated for the areas of **PVT3** plane and molecule projection, respectively. Considering the estimated area of a **PVT3** molecule, the determined limiting area indicates formation of **PVT3** molecule stacks with heights of more than ten molecules. The stacks originate from the **PVT3** aggregation at the air–water interface, which is also supported by the results from atomic force microscopy (AFM) experiments. The AFM imaging for a 70 mol% **PVT3** film reveals oval **PVT3** aggregates with heights about 40 nm distributed unevenly over the **PVT3**-rich area (Figure 4.2) [I]. Due to their non-amphiphilic nature, **PVT3** molecules form at the air–water interface a highly heterogeneous film with thickness more than one molecular layer. Relative surface coverages of the **PVT3** and ODA domains are roughly 90 and 10 %, respectively, in a 70 mol% **PVT3** film estimated from the AFM figure.

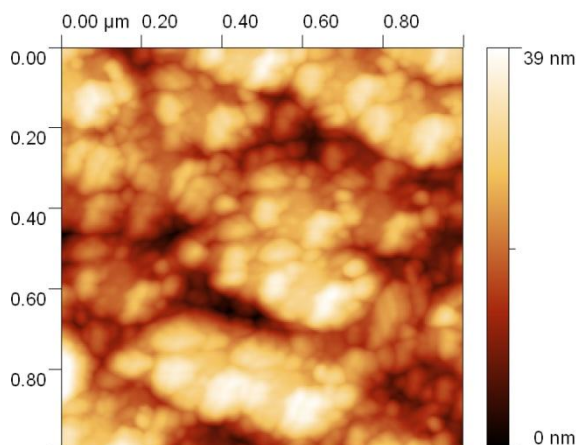


Figure 4.2. Atomic force microscopy imaging for a 70 mol% **PVT3** film on a glass substrate.

The LB film formation of the dyads has been studied earlier [V]. The relative dyad coverage in the monolayers (similar to those used in this study) with high molar fraction of the ODA matrix is roughly 50 %. The AFM imaging for the dyad monolayers showed extremely flat films with dyad molecules inhomogeneously distributed over the film area [V].

The absorption spectra for LB layers of the studied compounds are shown in Figure 4.3. The molar fractions of ZnDHD6ee, DHD6ee, **PVT3**, and **PHT** [147] were 18, 10, 70, and 60 mol%, respectively, in the ODA matrix. The **PPQ** and **TBD6a** layers were deposited by the LS method as 100 % films. The absorption maximum of the dyads around 430 nm (Figure 4.3a) corresponds to the porphyrin Soret band (transition $S_0 \rightarrow S_2$). The **PVT3** layer has a rather broad and strong absorption band with the maximum at 411 nm (Figure 4.3b) increasing light harvesting substantially at the wavelengths less than 500 nm [I]. Absorption spectra of the **PVT3** layers differ from each other by their amplitude [I,IV] showing weak reproducibility of the **PVT3** LB deposition. Each **PVT3** layer has an individual molecule aggregation and that causes the absorption differences.

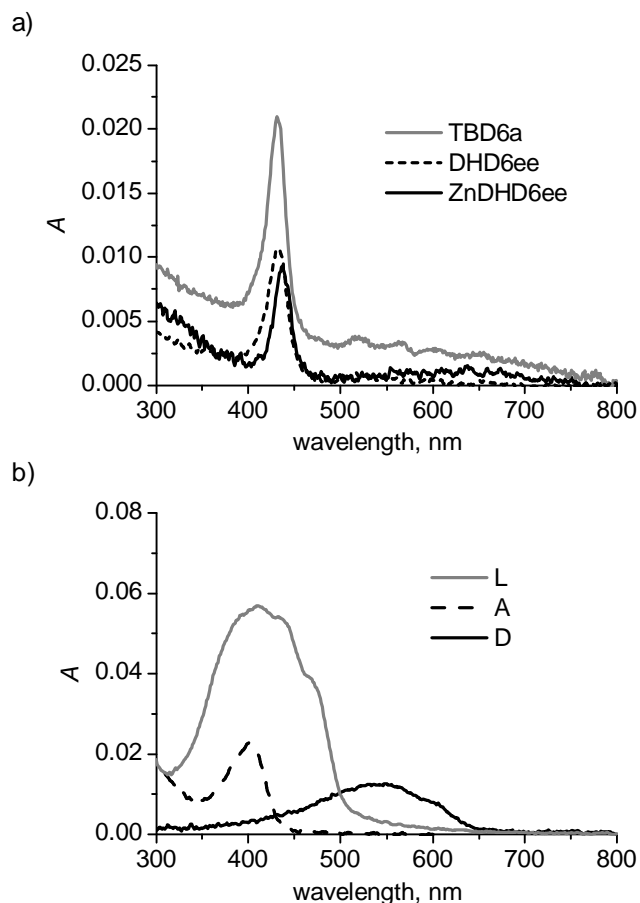


Figure 4.3. Absorption spectra of the (a) porphyrin–fullerene dyads, (b) **PVT3 (L)** and **PHT (D)** LB layers, and the **PPQ (A)** LS layer used in the studied films.

4.1.2. Spin-coated films

The **ZnPH4** layer was deposited by the spin-coating method, as well as the **PHT** layer in the samples with **ZnPH4**. The porphyrin–fullerene dyad on **ZnPH4** was deposited by the LB method as 10 mol% DHD6ee monolayer. The absorption spectra of the spin-coated **ZnPH4** and **PHT** layers are presented in Figure 4.4. The absorption bands of **ZnPH4** around 400 and 710 nm correspond to the phthalocyanine Soret (transition $S_0 \rightarrow S_2$) and Q ($S_0 \rightarrow S_1$) bands, respectively.

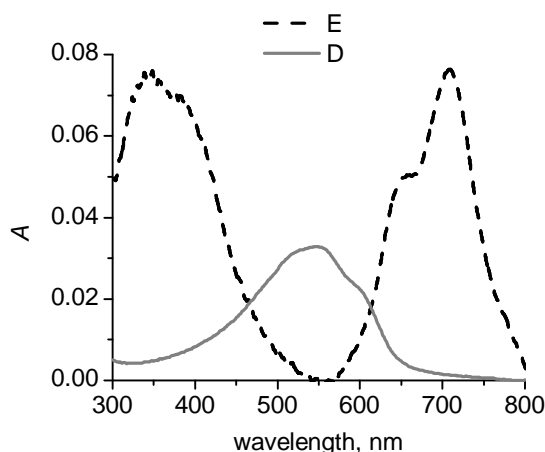
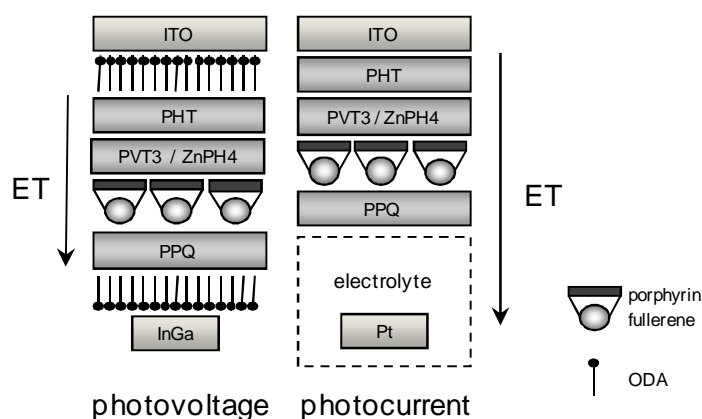


Figure 4.4. Absorption spectra of the spin-coated **ZnPH4** (**E**) and **PHT** (**D**) layers used in the studied films.

4.1.3. Layer arrangement in model cells

The porphyrin–fullerene dyad monolayer was deposited with the porphyrin moiety towards the substrate (substrate|porphyrin–fullerene) in the samples initiating the electron movement away from the substrate. The electron donating (including **PVT3**) and accepting layers were deposited to support the CS started by the dyad. The layer arrangement of each compound in the samples is illustrated visually in Chart 4.1. The PV and PC amplitudes are negative if the ET takes place to the desired vertical direction in the studied films.

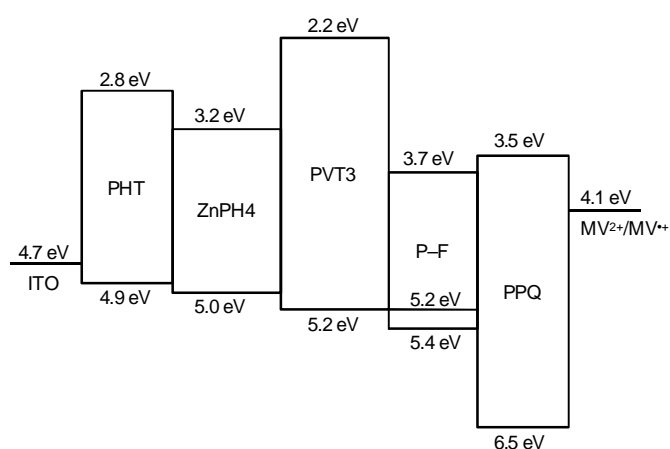
Chart 4.1. Layer arrangement of model cells in the photovoltage and photocurrent experiments. The layer order was same in the spectroscopic studies. Arrows show the direction of the electron transfer in the films.



The schematic energy level diagram of the studied compounds and the model photovoltaic cells is shown in Chart 4.2. Energy levels of ITO [148], **PHT** [149], **PPQ** [135], and MV^{2+} [150] are taken from the literature. Oxidation potential of **PVT3**, as well as

oxidation and reduction potentials of the dyads and **ZnPH4** were defined by differential pulse voltametry in solution. Reduction potential of **PVT3** was determined by subtracting the band gap (circa 3.0 eV from the absorption spectrum) from the oxidation potential. The oxidation and reduction potentials correspond to the HOMO and LUMO levels, respectively, of the compounds.

Chart 4.2. Schematic energy level diagram of the studied compounds and the model photovoltaic cells. Two HOMO levels of the porphyrin–fullerene dyad correspond to those of the **P** (5.4 eV) and **ZnP** (5.2 eV) moieties of the DHD6ee and ZnDHD6ee dyads, respectively. The LUMO level of the dyads corresponds to that of the fullerene moiety.



The secondary electron donation from **PHT**, **PVT3**, and **ZnPH4** to the porphyrin cation is supported by the higher (or equal) HOMO levels of the donors compared to the oxidation potentials of the dyads. This level is free in the porphyrin cation moiety of the dyad in the CS state. Similarly, the higher HOMO level of the next electron donor with respect to the previous one in the layer sequence supports the hole transfer towards the ITO electrode. The HOMO levels of the donors are lower than the work function of ITO supporting the hole transfer to ITO via the organic layers.

The ET from the fullerene anion to MV^{2+} is supported by the higher LUMO level of the fullerene moiety of the dyad compared to the reduction potential of MV^{2+} . The LUMO and HOMO levels of the donors are higher than those of **P-F** supporting the energetically favourable ET from excited donors to fullerene. Similarly, high LUMO levels of the donors hinder electron movement towards the ITO electrode. The ET from the fullerene anion to **PPQ** is not energetically favourable due to the higher LUMO level of **PPQ**. As earlier, the higher HOMO and LUMO levels of **PHT** compared to those of **ZnPH4** support electron donation from **PHT** to **ZnPH4**.

4.2. Energy transfer

Since fluorescence of a **PVT3** (= **L**) film covers the Q band absorption of the studied porphyrin–fullerene dyads, and is partly quenched in the presence of the dyad monolayer, interlayer ENT from excited **PVT3** to the dyad can be assumed [I]. To enable an efficient energy donation from **PVT3** to porphyrin, **PVT3** was deposited adjacent to the porphyrin moiety of the dyad to construct a **PVT3|P-F** (= **LP-F** film) bilayer sequence. The **PVT3** and **P-F** single layers were measured as references. Photoinduced ENT was mainly studied by the spectroscopic time-resolved absorption and fluorescence techniques [I,IV]. The transient absorption and fluorescence characteristic of the **P-F** monolayer are presented in detail in papers II and V, respectively.

The time-resolved fluorescence decays of the **LP-F** and **L** films obtained from the TCSPC experiments are shown in Figure 4.5. The rate constants determined from the three-exponential fit of the decays are presented in Table 4.1. Fluorescence decays for these molecules in solution follow the mono-exponential recombination dependence. In the case of a film, three exponents were needed for a good fit quality. This shows that the molecules have inhomogeneous surroundings in the studied films, but there is no real physical meaning for the components needed for fitting. The **P-F** monolayer in the film structure decreases the lifetimes of the fastest and the second-fastest **PVT3** fluorescence components circa 7.5 and 1.5 times, respectively, when mainly **PVT3** is photoexcited (Table 4.1). Shorter time constants of the **LP-F** film demonstrate the emission quenching in the presence of **P-F** monolayer. Quenched **PVT3** fluorescence supports the assumption of ENT between the layers, although it cannot be distinguished from the interlayer ET.

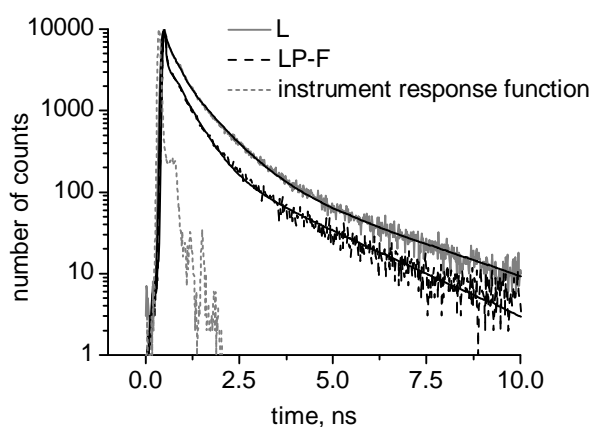


Figure 4.5. Time-resolved fluorescence decays of the **PVT3** and **PVT3|P-F** films for monitoring at 510 nm ($\lambda_{\text{ex}} = 404$ nm). The solid curves correspond to the three-exponential fits.

Table 4.1. Fluorescence lifetimes, τ_i , and pre-exponential factors, a_i , of the **PVT3** and **PVT3|P-F** films obtained from the exponential fit of the fluorescence decays in Figure 4.5.

Film	L	LP-F
τ_1 (ps)	180	24
a_1	0.146	0.286
τ_2 (ps)	730	440
a_2	0.080	0.086
τ_3 (ps)	2810	2060
a_3	0.004	0.004

The time-resolved absorption spectra from the flash-photolysis experiments of the **LP-F**, **L**, and **P-F** films for excitation at 355 nm are compared to each other in Figure 4.6. The broad transient absorption of the **PVT3** single layer with the maximum at 620 nm is assigned to the triplet state of thiophene derivative [151,152]. The transient absorption of **PVT3** triplet is quenched roughly to half in the presence of **P-F** monolayer (Figure 4.6). Quenching cannot be explained only by the 34 % lower absorption of the bilayer structure [IV], and therefore it supports the hypothesis of an interaction between the molecular layers after the photoexcitation. The photoinduced ENT in the **LP-F** structure can be described as a projection of the transfer on perpendicular to the plane of the molecular film:



where the star describes the site of excitation.

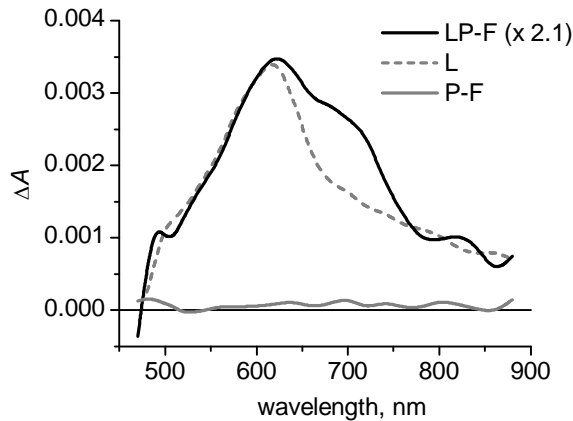


Figure 4.6. Time-resolved absorption spectra of the **PVT3|P-F** film and its corresponding single layers at 5 μs delay time ($\lambda_{\text{ex}} = 355$ nm). Note the magnification factor of the bilayer spectrum used to ease the comparison between the **PVT3|P-F** and **PVT3** spectra.

The time-resolved spectrum of the bilayer is not a sum of its components even if the shape is dominated by the **PVT3** triplet absorption, demonstrating photoinduced interaction between the **PVT3** and **P-F** layers. For excitation at 355 nm, mostly **PVT3** is photoexcited (Figure 4.3) and no transient bands of dyad should appear, as can be seen from the **P-F** spectrum in Figure 4.6, unless **PVT3** transfers its excitation energy to porphyrin. The transient absorption bands of the **LP-F** film at 490 and around 700 nm are not observed for the **PVT3** single layer, and are much stronger than those of the dyad monolayer. Both bands correspond to the transient bands of porphyrin cation of the dyad [II], assigning them for **P⁺** in the bilayer film. The transient absorption of porphyrin cation on the **LP-F** spectrum demonstrates the interlayer ENT to **P-F**, which is then followed by the primary ET from porphyrin to fullerene producing the porphyrin cation moiety. As discussed earlier, the quenched **PVT3** fluorescence and transient absorption in the presence of **P-F** support the hypothesis of the ENT as well.

The increased transient absorption of the **LP-F** film around 820 nm is assigned to the **PVT3** radical cation [151–153] and will be discussed in chapter 4.3.1.

4.3. Electron transfer

Photoinduced intermolecular ET in complex multilayer film structures was studied by the time-resolved PV and flash-photolysis techniques. The results from both measurement methods were combined to characterize the CT processes in the films.

4.3.1. *PVT3 as electron donor to porphyrin–fullerene dyad*

To study **PVT3** as a secondary electron donor to a porphyrin–fullerene dyad, the **PVT3|P-F** film sequence, similar to that used to study ENT in chapter 4.2, was investigated. The corresponding single layers were measured as references. The PV responses of the **P-F** and **LP-F** films for excitation at 436 nm (both **P** and **PVT3** chromophores are photoexcited), as well as that of a **PHT|PVT3|P-F** (= **DLP-F**) structure, are shown in Figure 4.7 [I]. The relative PV amplitudes (U_{out}) and the signal half-lives ($\tau_{1/2}$) for the studied films composed of the **PHT**, **PVT3**, **PPQ**, and **P-F** layers are presented in Table 4.2 [I]. However, the role of **PHT** and **PPQ** to the ET reactions will be discussed in detail in sections 4.3.2 and 4.3.3, respectively. The half-lives were determined from a power-law $U(t) \sim t^{-\beta}$ [154,155] fit of the PV decays, although in the complex films the CR followed it poorly [I].

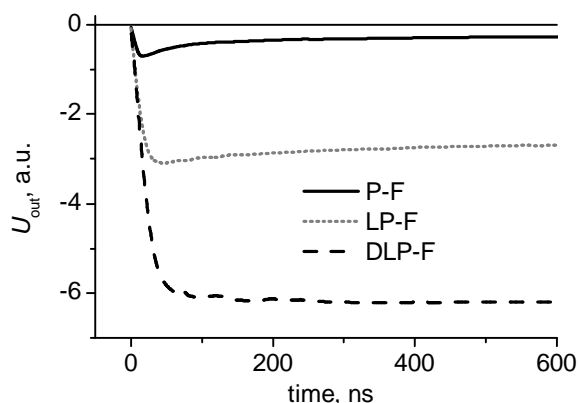


Figure 4.7. Time-resolved photovoltage responses of the **P-F**, **PVT3|P-F**, and **PHT|PVT3|P-F** films.

Table 4.2. Relative photovoltage amplitudes (U_{out}) and half-lives ($\tau_{1/2}$) for the studied film structures composed of the **P-F**, **PHT**, **PVT3**, and **PPQ** layers (λ_{ex} = 436 nm).

Film	U_{out} , a.u.	$\tau_{1/2}$, s
ITO P-F	1	9.2×10^{-7}
ITO LP-F	4.2	4.9×10^{-2}
ITO DLP-F	8.4	9.7
ITO P-FA	0.9	1.6
ITO LP-FA	9.3	4.0×10^{-2}
ITO DLP-FA	11.3	6.8
ITO L	0.6	2.8×10^{-2}
ITO D	0	–
ITO A	0	–

In the **LP-F** film, the PV amplitude is enhanced circa three times compared to the amplitude sum of the corresponding single layers (Table 4.2) indicating increased distance of charges and/or increased number of the CS states. Since signal decay for the **LP-F** film is fast right after the excitation, same as for the dyad monolayer, the primary decay process in the bilayer is assigned to the CR between the porphyrin and fullerene moieties. Signal half-life for the **LP-F** film is, however, 4-orders of magnitude longer than that for the dyad alone.

The increased PV amplitude and the fast primary decay process in the **LP-F** film are, at least partly, ascribed to the ENT from **PVT3**, which is then followed by the ET from porphyrin to fullerene, and finally the CR. Similarly, the enhanced PV amplitude and the prolonged signal half-life are assigned to the increased CS distance, i.e. to the secondary ET from **PVT3** to the porphyrin radical cation. The increased CS lifetime is produced by the longer distance between the positive and negative charges containing the lateral charge

hopping in the corresponding molecular networks as well. In addition, the slow signal decay for the **LP-F** film is also partly affected by the slow PV recombination in the **PVT3** single layer.

The normalized time-resolved absorption spectra of the **LP-F**, **DLP-F**, and **L** films for excitation at 430 nm are presented in Figure 4.8 [IV]. Both **PVT3** and **P-F** are photoexcited at the excitation wavelength used. The **PVT3** triplet absorption with the maximum at 620 nm dominates the spectral shape of the films. If the **LP-F** transient spectra with excitation at 355 nm (Figure 4.6) is compared with excitation at 430 nm, the increased absorption above 650 nm and the weaker band of porphyrin cation at 490 nm are observed for the 430 nm excitation. The increased absorption above 650 nm is assigned to the **PVT3** cation [151–153], but may also be affected by the porphyrin cation absorption. Thus, in the case of dyad photoexcitation at 430 nm, the secondary ET from **PVT3** to **P⁺** after the primary CS in the dyad is more pronounced.

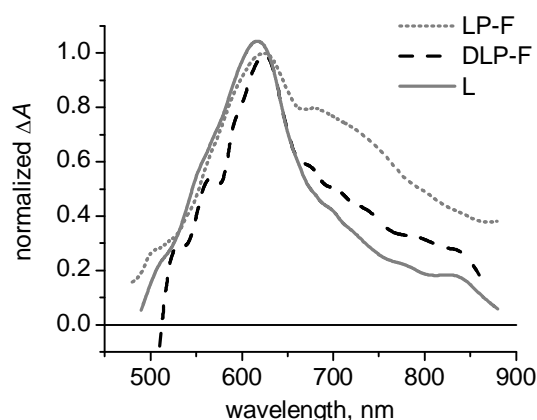
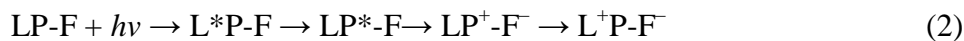
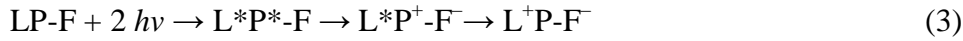


Figure 4.8. Normalized time-resolved absorption spectra of the **PVT3|P-F**, **PHT|PVT3|P-F**, and **PVT3** films at 5 μ s delay time ($\lambda_{\text{ex}} = 430$ nm).

The results obtained from both PV and flash-photolysis experiments support the ET from **PVT3** to **P⁺-F⁻**. If the electron and energy transfers are described as transfers perpendicular to the plane of the molecular film and the individual vertical steps contain the lateral migration of charges as well, the photoinduced reactions in the **LP-F** sequence for excitation at 355 nm (Eq.2) and at 430 nm (Eq. 3) can be presented as follows:



and



In $\text{L}^*\text{P}^*\text{-F}$ and $\text{L}^*\text{P}^+\text{-F}^-$ excitation is not obligatory on the neighboring **L** and **P-F** but within the migration distance. In the final transient CS state the positive charges are located in the **PVT3** network and the electrons in the fullerene sublayer.

4.3.2. PHT as electron donor

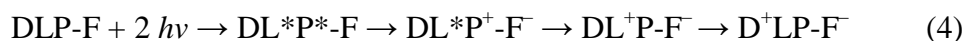
The film sequence **DLP-F** was measured to study the charge migration from **PHT** to **P-F** through the **PVT3** layer. Since **PHT** was demonstrated of being able to donate electrons to **PVT3** [I,IV], the CT through the whole film structure was expected yielding the final transient state $\text{D}^+\text{LP-F}^-$, in which the positive charges are located in the **PHT** layer and the electrons in the fullerene sublayer.

The time-resolved PV response of the **DLP-F** film is presented in Figure 4.7. Introducing **PHT** to the layer structure increased the PV amplitude two times compared to that of the **LP-F** film and prolonged the signal half-live to a time domain of seconds (Table 4.2). The PV amplitude of the **PHT** single layer is negligible for excitation at 436 nm. The enhanced PV amplitude is now assigned only to the extended CS distance due to the electron donation from **PHT** to the **PVT3|P-F** part of the film. The long CS distance together with the lateral charge migration in the corresponding layers produces the slower CR in such a complex film. The CR is hindered because back reaction can happen only when electrons and holes locate vertically next to each other.

Vertical charge migration through the layers explains also the slow signal rise for the **DLP-F** layer sequence (Figure 4.7).

The normalized time-resolved absorption spectrum of the **DLP-F** film is shown in Figure 4.8 [IV] together with the spectra of the **LP-F** and **L** films. Obvious differences in the transient spectra are observed when more functional layers are added to the film structure. The decreased transient absorption of the multilayer **DLP-F** film above 650 nm, if compared to the **LP-F** sample, can be assigned to the missing absorption of **PVT3** cation. **PVT3** acts as energy and electron donor to the dyad, as concluded earlier, but recombines back to the ground state via the interlayer ET from **PHT**. The increased transient absorption intensity of the **DLP-F** film above 650 nm, if compared to that of the **PVT3** single layer, is now assigned to the **PHT** cation [II]. Similarly, the decreased absorption below 620 nm is assigned to the **PHT** ground state bleaching caused by formation of the **PHT** cation. Only

the transient absorption of **PHT** cation and **PVT3** triplet can be resolved from the **DLP-F** spectrum, as could be expected if charge migration through the whole film is assumed. Considering the results obtained from both the PV and flash-photolysis measurements, the photoinduced CT reactions in the **DLP-F** film for excitation close to 430 nm can be presented as follows:



Summarizing, in **DL*P*-F** excitation is not obligatory on the neighboring **L** and **P-F**. After formation of the primary CS state **DLP⁺-F⁻**, the electron donation from **PVT3** and/or **PHT** to both porphyrin and **PVT3** radical cations takes place, producing the final transient CS state of **D⁺LP-F⁻** where the positive charges are located in the **PHT** layer and the negative charges in the fullerene sublayer.

4.3.3. *PPQ as electron acceptor from fullerene*

Film sequences of **P-F|PPQ** (= **P-FA**), **PVT3|P-F|PPQ** (= **LP-FA**), and **PHT|PVT3|P-F|PPQ** (= **DLP-FA**) were investigated to study the ET from the fullerene radical anion to **PPQ** polymer. The PV amplitudes and the signal half-lives of the films are shown in Table 4.2. The signal amplitudes of the **P-F** and **P-FA** films are approximately the same, whereas the signal decay is substantially slower for the sample with **PPQ**. The CS half-life is increased, but not the distance between the charges or the number of CS states indicating that the ET from the fullerene anion to **PPQ** is not efficient enough to increase the PV amplitude. In the **P-FA** film, the amplitude is controlled by the fast recombination of the primary CS in **P-F**, while the decay by the **PPQ** layer.

The PV responses of the **DLP-F** and **DLP-FA** films in microsecond timescale for excitation at 436 nm are presented in Figure 4.9 [I]. The signal for the film with **PPQ** is immediately after the excitation more intense, but decays considerably faster compared to the structure in the absence of **PPQ**. The signal amplitudes at 300 μs after the excitation are the same for both films, and therefore independent of presence or absence of the **PPQ** layer. Thus, the fullerene anion donates an electron to **PPQ**, but the recombination is fast and independent of the CT processes taking place in other parts of the film. Delayed recombination of the primary CS in **P-F** (due to the secondary ET reactions) increases the probability of ET from **F⁻** to **PPQ**. The PV signal half-life of the **LP-FA** film is slightly decreased, as is also the case with the **DLP-FA** sample, compared to the similar films

without **PPQ** (Table 4.2) indicating similar behavior in the samples with **PPQ** as an electron acceptor from the fullerene anion. The fast CR from **PPQ** indicates weak charge migration in the polymer, i.e. rather poor electron conducting properties of the **PPQ** layer.

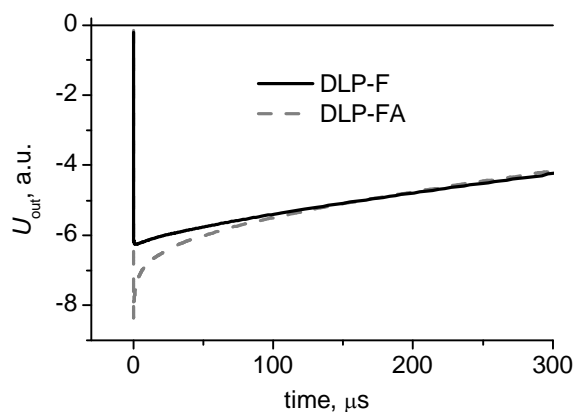


Figure 4.9. Time-resolved photovoltage responses of the **PHT|PVT3|P-F** and **PHT|PVT3|P-F|PPQ** films in microsecond timescale.

4.3.4. *ZnPH4 as electron donor to porphyrin–fullerene dyad*

To study the interlayer ET from **ZnPH4** (= **E**) to a porphyrin–fullerene dyad, a **ZnPH4|P-F** (= **EP-F**) film was measured [III,IV]. The corresponding single layers were measured as references. The PV responses of the **E** and **EP-F** films for excitation at 430 nm are shown in Figure 4.10. The relative PV amplitudes of the studied films when either both **ZnPH4** and porphyrin chromophores ($\lambda_{\text{ex}}=430$ nm) or exclusively **ZnPH4** ($\lambda_{\text{ex}}=710$ nm) are excited, are presented in Table 4.3.

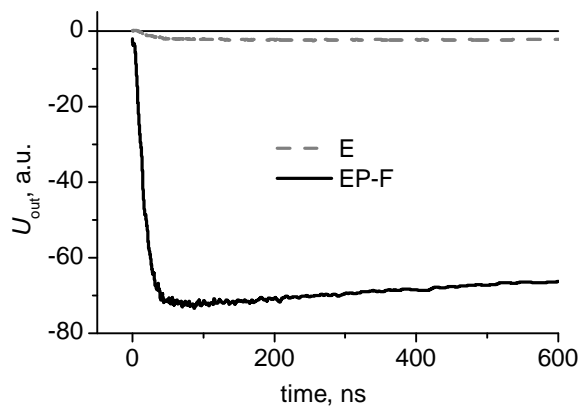


Figure 4.10. Time-resolved photovoltage responses of the **ZnPH4** and **ZnPH4|P-F** films.

Table 4.3. Relative photovoltage amplitudes (U_{out}) of the **P-F**, **ZnPH4**, and **ZnPH4|P-F** films for excitation at 430 and 710 nm.

Film	U_{out} , a.u.	
	430 nm	710 nm
ITO P-F	1	0
ITO E	6.5	1
ITO EP-F	184.2	2.8

If the porphyrin and phthalocyanine chromophores are both excited, the PV amplitude of the **EP-F** film is enhanced 25-fold compared to the amplitude sum of the corresponding single layers. If only **ZnPH4** is excited, the amplitude is three times higher than that of **ZnPH4** alone. To explain the increased PV amplitudes of the **EP-F** structure, two possible CT mechanisms can be considered corresponding to the excitation at 430 nm (Eq. 5 and 6) and at 710 nm (Eq. 6):



Higher amplitude obtained for the bilayer **EP-F** film is due to the ET from **E** to **P** that is followed by formation of the $\text{E}^+\text{P-F}^-$ state, yielding the longer distance between the negative and positive charges. In the final CS state the positive charges are located in the **ZnPH4** layer and the electrons in the fullerene sublayer. The interaction between excited **ZnPH4** and ground state **P-F** is weak, as will be discussed in detail later, excluding the ENT from **ZnPH4** to porphyrin. The ENT from porphyrin to phthalocyanine is demonstrated in the literature [71] and may take place in the studied systems as well.

In the studied samples, the **EP-F** film absorbs roughly three times more photons when excited at 710 nm compared to that at 430 nm [III]. Assuming only ET from excited **ZnPH4** to the dyad (as well as the ENT from porphyrin to **ZnPH4** in the case of porphyrin photoexcitation), three times higher PV amplitude could be expected for excitation at 710 nm. The amplitude is, however, two times lower if only **ZnPH4** is excited indicating that the reaction (5) is six times more efficient than the reaction (6). Therefore, the efficiency of interlayer ET from excited **ZnPH4** to fullerene via the porphyrin moiety of the dyad at ground state is rather poor. The extremely high PV amplitude of the **EP-F** film for excitation at 430 nm (Table 4.3) can be explained only by the enhanced CS efficiency in the bilayer

structure with the excited dyad, and thus demonstrating the crucial role of the primary ET in **P-F** for the overall CS efficiency in such a molecular system.

The PV decays for the films with **ZnPH4** did not follow the power-law. However, one can see from the graphs that the PV decay of the **EP-F** structure is slower compared to those of the **E** and **P-F** single layers at both excitation wavelengths [III], although the $\tau_{1/2}$ values were not determined. As earlier, the increased PV amplitude and the prolonged CS lifetime of the bilayer can be explained by the vertical interlayer ET and the lateral charge hopping in the corresponding layers.

The time-resolved absorption spectra of the **EP-F**, **E**, and **P-F** films for excitation at 430 nm are shown in Figure 4.11. The transient spectrum of the **EP-F** film is not a sum of its components demonstrating interaction between the layers in excited state. The absorption bleaching of the **ZnPH4** single layer below 550 nm and at 750 nm corresponds to the wavelengths of phthalocyanine ground state absorption (Figure 4.4). The transient absorption of **ZnPH4** at 620 nm is assigned to the phthalocyanine triplet state.

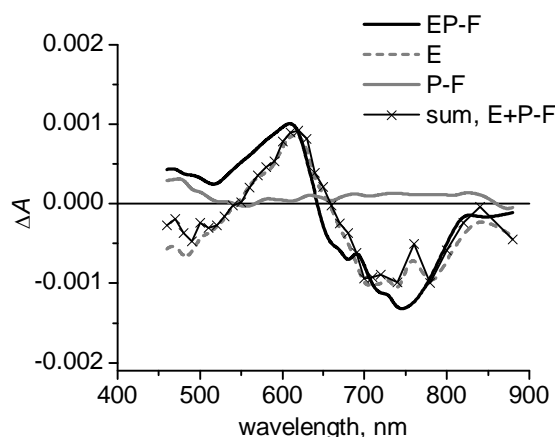


Figure 4.11. Time-resolved absorption spectra of the **ZnPH4|P-F**, **ZnPH4**, and **P-F** films, as well as the sum of **ZnPH4** and **P-F** spectra at 5 μ s delay time ($\lambda_{\text{ex}}=430$ nm).

The increased transient absorption of the **EP-F** film below 620 nm is the most obvious difference between the spectra of the films with and without the dyad monolayer. The absorption below 620 nm is assigned to the **ZnPH4** radical cation since it is not observed for the **E** single layer, and it does not correspond to the porphyrin cation absorption. If only **ZnPH4** is excited at 720 nm, the time-resolved absorption spectra of the **E** and **EP-F** films are identical [IV] supporting the weak interaction between the excited **ZnPH4** and the non-excited dyad.

The results from the flash-photolysis studies support the conclusions made from the PV measurements demonstrating the crucial role of the primary ET in porphyrin–fullerene dyad for the overall CT efficiency in a bilayer cell with **ZnPH4** and **P-F**. Thus, the electron donation from **ZnPH4** to **P-F** (Eq. 6) is rather inefficient compared to that from **ZnPH4** to **P⁺-F⁻** (Eq. 5), as was already supposed in the PV discussion.

4.4. Photocurrent

The photovoltaic characteristics of the model photocells were studied using the electrochemical PC technique [I,III]. Series of molecular film structures, similar to those used in the PV and flash-photolysis experiments were deposited directly onto ITO electrode for the PC measurements.

4.4.1. Step-wise photocurrent

The step-wise light-on/off PC responses of the **P-F**, **DP-F**, and **DLP-F** films are shown in Figure 4.12. The PC amplitudes (I_{pc}) with zero bias voltage for the cells composed of the **P-F**, **PHT**, **PVT3**, and **PPQ** layers are presented in Table 4.4. The PC amplitudes increase with the number of single functional layers as far as fullerene is in contact with the electrolyte. The PC amplitude for the **DP-F** film is roughly two times higher than that of **P-F** alone. Adding **PVT3** to the cell structure to construct the **DLP-F** layer sequence further enhanced the PC generation about 3.5 times.

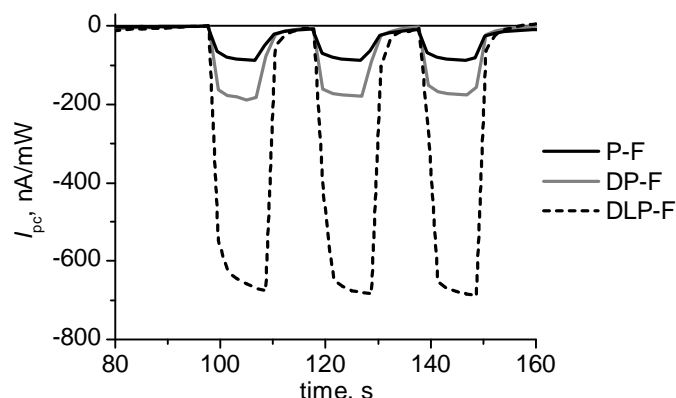


Figure 4.12. Step-wise photocurrent responses of the **P-F**, **PHT|P-F**, and **PHT|PVT3|P-F** films for excitation at 436 nm.

Table 4.4. Measured and relative photocurrent amplitudes (I_{pc}) for the films composed of the **P-F**, **PHT**, **PVT3**, and **PPQ** layers ($\lambda_{ex}= 436$ nm). Two **PHT** or **PVT3** bottom layers (marked by one **D** or **L**) had to be used in the **DP-F**, **LP-F**, **DP-FA**, and **LP-FA** films due to the technical deposition reasons.

Film	I_{pc} , nA/mW	I_{pc} , a.u.
ITO P-F	90	1
ITO DP-F	190	2.1
ITO LP-F	700	7.8
ITO DLP-F	690	7.8
ITO P-FA	20	0.2
ITO DP-FA	130	1.4
ITO LP-FA	340	3.8
ITO DLP-FA	250	2.8
ITO L	390	4.3
ITO D	50	0.6
ITO A	30	0.3

The PC amplitudes for the **LP-F** and **DLP-F** films are approximately equal (Table 4.4), although the absorbance of the former is only half from that of the **LP-F** film at the excitation wavelength, showing the higher PC yield for the sample with more functional layers. Furthermore, the PC generation of the multilayer structures (excluding the films with **PPQ**) is higher than the sum of currents of the corresponding components, i.e. the PC is enhanced because of the improved CS, rather than solely due to the increased photon harvesting. The increased absorbance together with the long-lived CS enhance the PC response of the multicomponent photocells.

The multilayer films with **PPQ** produced high PV amplitudes (Table 4.2), but the result is opposite in the PC measurements (Table 4.4) [I]. The PC generation for the cells with **PPQ** in contact with the electrolyte is weak compared to the similar films in the absence of **PPQ**. The conclusion about the weak electron migration in the **PPQ** layer made on the basis of the PV experiments in section 4.3.3 is now supported by the results from the PC measurements, demonstrating the poor electrical conductivity of **PPQ**. It seems that **PPQ** is not useful as an electron acceptor layer in such photovoltaic assemblies.

The step-wise light-on/off PC responses of the **PHT|ZnPH4|P-F** (= **DEP-F**), **ZnPH4**, and **PHT|ZnPH4** (= **DE**) films for excitation at 710 nm are presented in Figure 4.13. The PC amplitudes for the cells composed of the corresponding layers are shown in Table 4.5 [III]. The **P-F** monolayer deposition onto the **E** or **DE** films decreases the PC generation at each excitation wavelength. The PC decrease for excitation at 540 nm (close to the maximum absorbance of **PHT**, Figure 4.4) and 710 nm is expected since the ET from

ZnPH4 to **P-F** was shown (by the PV and flash-photolysis experiments, section 4.3.4) to be efficient only in the case of the excited dyad. The non-excited dyad monolayer only creates a barrier for charge migration by increasing resistivity of the system.

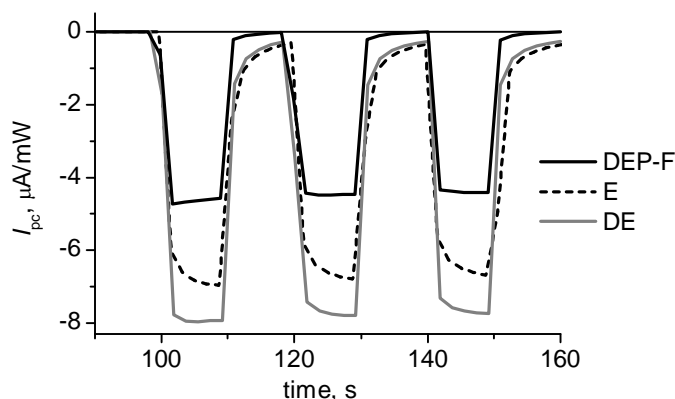


Figure 4.13. Step-wise photocurrent responses of the **PHT|ZnPH4|P-F**, **ZnPH4**, and **PHT|ZnPH4** films for excitation at 710 nm.

Table 4.5. Step-wise photocurrent amplitudes (I_{pc}) for the samples composed of the **P-F**, **ZnPH4**, and **PHT** layers for excitation at 430, 540, and 710 nm.

Film	I_{pc} , $\mu\text{A}/\text{mW}$		
	430 nm	540 nm	710 nm
ITO P-F	0.02	0	0
ITO E	0.56	0.24	6.98
ITO EP-F	0.52	–	1.60
ITO DEP-F	2.00	2.25	4.58
ITO DE	–	5.28	7.93
ITO D	0.35	0.79	0

In the case of photoexcited dyad at the excitation wavelength 430 nm, the decreased PC amplitudes for the films with the **P-F** monolayer (Table 4.5) can be explained by the weak electronic interaction between fullerene and electrolyte. The fullerene anion is energetically more stable than its ground state creating an energy trap for electrons [156]. Efficient ET from **ZnPH4** to $\text{P}^+\text{-F}^-$ was demonstrated in the PV experiments, and therefore the PC limiting step is the ET from the fullerene anion to electrolyte. However, the positive effect of the dyad monolayer to the PC generation was demonstrated for the multilayer films composed of the **PVT3**, **PHT**, and **P-F** LB layers [I]. Thus, it seems that the interaction between fullerene and electrolyte functions oppositely to the current generation for the films with rather high current amplitudes.

As shown in Figure 4.13 and Table 4.5, the highest PC amplitudes are obtained for the **DE** heterojunction. When **PHT** is photoexcited at 540 nm, roughly five times higher PC response is observed for the **DE** film compared to the amplitude sum of the corresponding single layers. The PC increase is lower if only **ZnPH4** is photoexcited at 710 nm, but still it is enhanced compared to that of the **ZnPH4** single layer. These observations demonstrate the efficient interlayer ET from **PHT** to **ZnPH4** regardless of the excited chromophore.

4.4.2. Action spectra and current–voltage curves

The current–voltage curves and incident photon to current efficiency spectra of the **DLP-F** and **DEP-F** films are presented in papers I and III, respectively, as well as the photovoltaic parameters obtained for the model photovoltaic cells.

The IPCE spectra for the samples in the absence of **PPQ** follow the absorption of the films demonstrating the importance of each functional layer to the photon harvesting efficiency, and thus to the PC efficiency as well [I]. The action spectra for the films with **PPQ** resemble the absorption spectrum of **PPQ** [I] showing its unsuitability for an electron acceptor layer in this kind of photoactive devices.

The effect of **PHT** on the **DEP-F** action spectrum is striking and stronger than can be predicted on the basis of the film absorption [III]. In contrast, the influence of **ZnPH4** on PC is weaker than could be expected. Thus, the ET from excited **PHT** to **ZnPH4** is more pronounced than that from **PHT** to excited **ZnPH4**.

The highest photovoltaic parameters are obtained for the **DE** heterojunction [III] demonstrating the efficient CS at the interface and rather good electrical properties of the **PHT** and **ZnPH4** layers. For the **DE** film, the internal quantum yield of PC is circa 20 % at the excitation wavelength 540 nm. The external quantum yield and the power conversion efficiency of the **DE** film are about 1.4 and 0.024 %, respectively, for excitation at 710 nm. The rather low fill factor values obtained for the model photocells (the best 24 % obtained for the **EP-F** film) show the need to overcome limiting factors of the charge transport through the system.

4.5. Electrical and optical signal decays

Photoinduced intermolecular ET in thin films with identical layer sequences was studied using the time-resolved electrical photovoltage [I,III] and optical flash-photolysis [II,IV] techniques. Both methods were utilized to follow the final transient CS state of the films, and thus the optical and electrical signal lifetimes should correlate with each other. The lifetime of spectroscopic signal is, however, shorter than that of the electrical signal [II,IV] as shown in Figure 4.14, in which normalized PV and flash-photolysis decays of the **LP-F** and **EP-F** films are compared. Same phenomenon was observed for all the studied layer sequences.

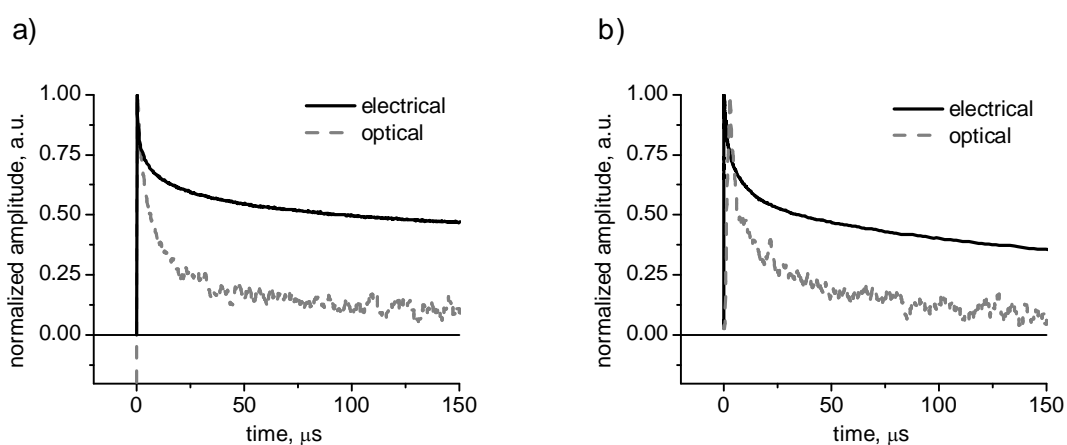


Figure 4.14. Normalized electrical (photovoltage) and optical (flash-photolysis) signal decays of the (a) **PVT3|P-F** and (b) **ZnPH4|P-F** films.

Shorter lifetime of the optical signal can be explained by the different measurement principles and phenomena taking place in the studied systems. The PV amplitude is sensitive to the number of positive and negative charges and to the distance between them, whereas spectroscopic signal is affected by the existence of molecular transient states. Thus, all charges in the film have influence to the electrical signal, even if they could not be detected by the spectroscopic methods. Extremely long-lived electron-hole pairs in the studied cells result from vertical and lateral charge migration in the corresponding molecular layers that may be followed by charge ejection to the molecular environment as “free” charges. Free charges are not bound to any specific molecular moieties, and thus they cannot be detected spectroscopically. Observed long-lived photovoltage responses (especially extremely long-lived tails of the photovoltage signals) are produced by this kind of free electron-hole pairs.

The charge ejection as free charges is more pronounced in complex films with long CS distance and efficient charge migration in the molecular layers. The intramolecular CS in the

P-F monolayer results in rather similar electrical and optical responses, since the fast CR enables only weak lateral charge hopping in the porphyrin and fullerene networks [IV].

4.6. Organic photovoltaic cell design

In the following discussion, further improvements to the photovoltaic performance of the model cells are considered.

The most organic photovoltaic cells to date are based on the bilayer or bulk heterojunction concept. The directionality of ET in a layered cell is reached by depositing active layers onto each other with respect to their energy levels and electrode work functions. In addition, difference between the HOMO and LUMO levels of donor and acceptor, respectively, affect together with the electrode work functions the maximum possible voltage produced by the cell. Due to the short exciton diffusion length and the low charge carrier mobility in organic electronic materials, the total cell thickness must be a compromise between the maximum absorbance and the minimum serial resistance. The maximum thickness of 100 nm has been typically considered as the upper limit for an organic photovoltaic cell.

In a layered device, the thickness of every functional layer has to be optimized with respect to other layers in order to reduce optical filtering and decrease the layer resistivity. The cell thickness in bulk heterojunction can be increased without decreasing the exciton dissociation yield due to the short separation of the donor and acceptor parts. However, the low charge mobility in organic materials limits the bulk heterojunction film thickness, and thus the absorbance cannot be increased indefinitely. Electrodes with different work functions are needed to enable symmetry breaking condition in the bulk heterojunction based devices.

To increase the conductivity of the films used in this study, the insulating ODA matrix should not be used. Impurities in the films typically act as charge traps reducing the charge mobility. To minimize the number of impurities in the film, only ultrapure compounds should be used (even commercial compounds may need further purification). Samples can be thermally treated in rather high temperatures to reduce number of charge traps such as holes and grain boundaries in the films.

To maximize the light harvesting of a photocell, the visible spectrum should be covered as completely as possible. This can be obtained by introducing the studied compounds **P-F**, **PVT3**, **PHT**, and **ZnPH4** to the cell structure. The **PHT|ZnPH4** heterojunction establishes

an efficient CS interface and it seems promising for photovoltaic applications. The high internal quantum yield of ET from **PHT** to **ZnPH4**, together with the broad absorption at the visible region enables efficient light-to-current conversion in such a device under the solar spectrum. Both compounds have good electron donating properties, and thus they provide an efficient hole transfer assembly next to anode. To further increase the light harvesting, **PVT3** can be included to the layer structure enhancing the absorption in blue region. The porphyrin–fullerene dyad can be utilized as an efficient CS interface.

Taking into account the energy levels of the compounds (Chart 4.2), a model layered photovoltaic cell could be constructed as ITO|**PHT**|**ZnPH4**|**PVT3**|**P-F** $\times n$ |2nd electrode. The number of **P-F** layers (n) should be optimized empirically. To further improve the cell performance and protect the **P-F** part of the sample, an electron accepting layer from the fullerene anion can be introduced to the film structure. The LUMO level of **PVT3** does not support in ground state the electron accepting from excited **ZnPH4**, but it may act as an electron acceptor from **ZnPH4** in its cationic state. The sample ITO|**PHT**|**ZnPH4**|**P-F** $\times n$ |electron acceptor|2nd electrode may work efficiently as well, since efficient ET from **ZnPH4** to **P-F** was demonstrated and the electron acceptor is used to provide a good electrical contact with the second electrode. In these model sample structures, **PHT** enables good electric contact with the ITO electrode and **PVT3** acts as a light harvesting layer in blue region. **ZnPH4** is used to increase absorbance at near IR region and establish efficient CS junction with **PHT**. The oriented **P-F** monolayer (deposited by the LB or LS method) is used to initiate the ET reactions to the desired vertical direction, i.e. from ITO towards the second electrode.

Bulk heterojunction concept can be introduced to the film structure in order to avoid the LB and LS deposition of the dyad. Bulk heterojunction can be combined with the bilayer concept to exploit the favourable properties of both device architectures. **PVT3** can be mixed with **P-F** to enable efficient energy donation and exciton dissociation in such a blend. This kind of bulk heterojunction can be combined with the bilayer concept to construct ITO|**PHT**|**ZnPH4**|**PVT3**+**P-F**|2nd electrode cell. To make the manufacturing easier and further improve the exciton dissociation, **PHT** and **ZnPH4** can be blended together as well, constructing ITO|**PHT**+**ZnPH4**|**PVT3**+**P-F**|2nd electrode cell. Furthermore, an electron accepting layer adjacent to the second electrode can be used to increase the cell efficiency. With the introduction of the bulk heterojunction concept to the cell design, the directionality of ET is partly lost but it is compensated by the enhanced absorption (or at least a possibility

to increase the film thickness) and exciton dissociation. Since in such samples each layer is spin-coated, the major problem is to find solvents suitable for the layer-on-layer deposition.

If the second electrode work function is lower than that of ITO (e.g. that of Au), the film structure should be reversed to attain the electron movement in the direction which is helped by the built-in electric field. Molecular oxygen has negative effect on both PC generation and stability in organic photovoltaic. Encapsulation is the method to protect photoactive layers and electrodes from oxygen and humidity. Promising studies of cell encapsulation have already been carried out [157,158].

4.7. Future perspectives

Organic solar cells have unlimited number of potential applications because of their possibility of being thin, flexible, and lightweight. Polymeric solar panels could be painted over rooftops and windows to enable solar energy harvesting. Such photovoltaic layers could also be printed on laptops and mobile phones to provide charger in the device itself, and thus enable continuous charging in light. These are only few examples for the optimistic future perspectives of organic photovoltaic.

However, many problems in organic photovoltaic must be overcome before these visions will be realized. The most crucial weaknesses of organic photovoltaic to date are poor power conversion efficiency and operating lifetime, as discussed earlier. These major problems need to be resolved before organic revolution may truly begin. This study was aimed to increase the knowledge on the fundamental physics of organic electronic systems. Increased understanding on the interaction of organic electronic materials can be used in designing new and more sophisticated organic photovoltaic applications in the future.

Organic materials capable of electric conduction can be utilized also in other applications than solar cells. Organic materials are already used to construct light emitting diodes [111,114]. Organic gas- and photo-sensors have been introduced as well [159,160]. The unique features of organic electronic materials create possibilities for new applications that would be impossible using traditional semiconducting materials or metals [161].

5. Conclusions

Intermolecular energy and electron transfers in organic multilayer thin films were studied. The photoinduced processes were characterized by constructing various layer sequences, which were then measured by mainly the time-resolved Maxwell displacement charge and flash-photolysis techniques. In addition, electrochemical photocurrent measurements were carried out to study the photovoltaic performance of the complex film structures. The results from each measurement method were combined in order to identify the photoinduced processes in the films. The samples were prepared by the Langmuir–Blodgett and spin-coating methods onto flat substrates.

The oriented porphyrin–fullerene dyad monolayer was utilized to initiate the electron transfer in perpendicular to the plane of the films. Excited phenyl vinyl thiophene derivative, **PVT3**, was demonstrated to perform both the energy and electron transfers to the porphyrin–fullerene dyad. The charge separation was further extended by depositing **PVT3** between hole conducting polymer poly(hexylthiophene), **PHT**, and the porphyrin moiety of the dyad yielding the final transient charge separated state, in which the holes are located in the **PHT** network and the electrons in the fullerene sublayer. In such a complex film structure, the lifetime of the electron transfer state was prolonged to a time domain of seconds due to the long charge separation distance and the lateral charge hopping in the corresponding molecular networks. The electron conducting property of *n*-type polymer poly(phenylene quinoxaline) derivative, **PPQ**, was found to be rather poor for such photovoltaic devices.

The crucial role of the excited dyad for the overall charge transfer efficiency in the model cells with phthalocyanine derivative, **ZnPH4**, as a secondary electron donor to the dyad was demonstrated. The electron donation from **ZnPH4** to the porphyrin cation was extremely efficient producing the **ZnPH4** cation and fullerene anion moieties. In addition, an efficient charge separation in a heterojunction composed of the **PHT** and **ZnPH4** layers was shown.

The electrical signal lifetime was longer than that of the optical signal for similar samples in same measurement conditions. The difference in decay times is explained by charge ejection to the molecular environment as the final transient state of the systems, generating the long-lived free charges that produce the electrical signal but are less pronounced in the optical signals.

The multistep electron transfer through the sandwich-like film structure producing the long-lived charge separated state can be utilized in the development of photoactive molecular devices such as photosensors and photovoltaic cells.

References

1. *Key World Energy Statistics 2007*, International Energy Agency, 2007, http://www.iea.org/textbase/nppdf/free/2007/key_stats_2007.pdf.
2. *Inventory of U.S. Greenhouse Gas Emissions and Sinks: 1990–2006*, U.S. Environmental Protection Agency, April 15, 2008, http://epa.gov/climatechange/emissions/downloads/08_CR.pdf.
3. Hermann, W. A. *Energy* **2006**, *31*, 1685.
4. Ohl, R. S. Light-Sensitive Electric Device, US Patent No. 2,402,622, 27th May, **1941**.
5. Ohl, R. S. Light-Sensitive Device Including Silicon, US Patent No. 2,443,542, 27th May, **1941**.
6. Green, M. A. *Sol. Energy* **2004**, *76*, 3.
7. Green, M. A. *Physica E* **2002**, *14*, 11.
8. Green, M. A. *Physica E* **2002**, *14*, 65.
9. Wang, Q.; Ito, S.; Grätzel, M.; Fabregat-Santiago, F.; Mora-Seró, I.; Bisquert, J.; Bessho, T.; Imai, H. *J. Phys. Chem. B* **2006**, *110*, 25210.
10. Grätzel, M. *Inorg. Chem.* **2005**, *44*, 6841.
11. Grätzel, M. *J. Photochem. Photobiol. A* **2004**, *164*, 3.
12. Hagfeldt, A.; Grätzel, M. *Acc. Chem. Res.* **2000**, *33*, 269.
13. Nazeeruddin, M. K.; Kay, A.; Rodicio, I.; Humphry-Baker, R.; Müller, E.; Liska, P.; Vlachopoulos, N.; Grätzel, M. *J. Am. Chem. Soc.* **1993**, *115*, 6382.
14. Koeppe, R.; Sariciftci, N. S.; Troshin, P. A.; Lyubovskaya, R. N. *Appl. Phys. Lett.* **2005**, *87*, 244102.
15. Nelson, J. *Mater. Today* **2002**, *5*(5), 20.
16. Brabec, C. J.; Sariciftci, N. S. *Mater. Today* **2000**, *3*(2), 5.
17. Kim, K.; Liu, J.; Namboothiry, M. A. G.; Carroll, D. L. *Appl. Phys. Lett.* **2007**, *90*, 163511.
18. Li, G.; Shrotriya, V.; Yao, Y.; Yang, Y. *J. Appl. Phys.* **2005**, *98*, 043704.
19. Sariciftci, N. S. *Mater. Today* **2004**, *7*(9), 36.
20. Spanggaard, H.; Krebs, F. C. *Sol. Energy Mater. Sol. Cells* **2004**, *83*, 125.
21. Gebeyehu, D.; Maennig, B.; Drechsel, J.; Leo, K.; Pfeiffer, M. *Sol. Energy Mater. Sol. Cells* **2003**, *79*, 81.
22. Gust, D.; Moore, T. A.; Moore, A. L. *Acc. Chem. Res.* **2001**, *34*, 40.

23. Wasielewski, M. R. *Chem. Rev.* **1992**, 92, 435.
24. D'Souza, F.; Ito, O. *Coord. Chem. Rev.* **2005**, 249, 1410.
25. Guldi, D. M.; Zilbermann, I.; Gouloumis, A.; Vázquez, P.; Torres, T. *J. Phys. Chem. B* **2004**, 108, 18485.
26. Fukuzumi, S.; Ohkubo, K.; Imahori, H.; Shao, J.; Ou, Z.; Zheng, G.; Chen, Y.; Pandey, R. K.; Fujitsuka, M.; Ito, O.; Kadish, K. M. *J. Am. Chem. Soc.* **2001**, 123, 10676.
27. Chukharev, V.; Tkachenko, N. V.; Efimov, A.; Guldi, D. M.; Hirsch, A.; Scheloske, M.; Lemmetyinen, H. *J. Phys. Chem. B* **2004**, 108, 16377.
28. Imahori, H.; Tkachenko, N. V.; Vehmanen, V.; Tamaki, K.; Lemmetyinen, H.; Sakata, Y.; Fukuzumi, S. *J. Phys. Chem. A* **2001**, 105, 1750.
29. Isosomppi, M.; Tkachenko, N. V.; Efimov, A.; Lemmetyinen, H. *J. Phys. Chem. A* **2005**, 109, 4881.
30. Schuster, D. I.; MacMahon, S.; Guldi, D. M.; Echegoyen, L.; Braslavsky, S. E. *Tetrahedron* **2006**, 62, 1928.
31. Imahori, H.; Sakata, Y. *Adv. Mater.* **1997**, 9, 537.
32. Kuciauskas, D.; Lin, S.; Seely, G. R.; Moore, A. L.; Moore, T. A.; Gust, D.; Drovetskaya, T.; Reed, C. A.; Boyd, P. D. W. *J. Phys. Chem.* **1996**, 100, 15926.
33. Echegoyen, L.; Echegoyen, L. E. *Acc. Chem. Res.* **1998**, 31, 593.
34. Guldi, D. M.; Prato, M. *Acc. Chem. Res.* **2000**, 33, 695.
35. Imahori, H.; Tamaki, K.; Guldi, D. M.; Luo, C.; Fujitsuka, M.; Ito, O.; Sakata, Y.; Fukuzumi, S. *J. Am. Chem. Soc.* **2001**, 123, 2607.
36. Currie, M. J.; Mapel, J. K.; Heidel, T. D.; Goffri, S.; Baldo, M. A. *Science* **2008**, 321, 226.
37. Thompson, B. C.; Fréchet, J. M. J. *Angew. Chem. Int. Ed.* **2008**, 47, 58.
38. Moliton, A.; Nunzi, J-M. *Polym. Int.* **2006**, 55, 583.
39. Li, G.; Shrotriya, V.; Huang, J.; Yao, Y.; Moriarty, T.; Emery, K.; Yang, Y. *Nat. Mater.* **2005**, 4, 864.
40. Kim, J. Y.; Lee, K.; Coates, N. E.; Moses, D.; Nguyen, T-Q.; Dante, M.; Heeger, A. J. *Science* **2007**, 317, 222.
41. Goetzberger, A.; Hebling, C.; Schock, H-W. *Mater. Sci. Eng. R* **2003**, 40, 1.
42. Günes, S.; Neugebauer, H.; Sariciftci, N. S. *Chem. Rev.* **2007**, 107, 1324.
43. Hoppe, H.; Sariciftci, N. S. *J. Mater. Res.* **2004**, 19, 1924.
44. Gregg, B. A. *J. Phys. Chem. B* **2003**, 107, 4688.

45. Brabec, C. J.; Sariciftci, N. S.; Hummel, J. C. *Adv. Funct. Mater.* **2001**, *11*, 15.
46. Saunders, B. R.; Turner, M. L. *Adv. Colloid Interface Sci.* **2008**, *138*, 1.
47. Günes, S.; Fritz, K. P.; Neugebauer, H.; Sariciftci, N. S.; Kumar, S.; Scholes, G. D. *Sol. Energy Mater. Sol. Cells* **2007**, *91*, 420.
48. Klein, C.; Nazeeruddin, Md. K.; Liska, P.; Di Censo, D.; Hirata, N.; Palomares, E.; Durrant, J. R.; Grätzel, M. *Inorg. Chem.* **2005**, *44*, 178.
49. Gregg, B. A. *Coord. Chem. Rev.* **2004**, *248*, 1215.
50. Greenham, N. C.; Peng, X.; Alivisatos, A. P. *Phys. Rev. B* **1996**, *54*, 17628.
51. Dimroth, F. *Phys. Stat. Sol.* **2006**, *3*, 373.
52. Hegedus, S. *Prog. Photovoltaics Res. Appl.* **2006**, *14*, 393.
53. Ghosh, A. K.; Morel, D. L.; Feng, T.; Shaw, R. F.; Rowe Jr., C. A. *J. Appl. Phys.* **1974**, *45*, 230.
54. Waldauf, C.; Scharber, M. C.; Schilinsky, P.; Hauch, J. A.; Brabec, C. J. *J. Appl. Phys.* **2006**, *99*, 104503.
55. Xue, J.; Uchida, S.; Rand, B. P.; Forrest, S. R. *Appl. Phys. Lett.* **2004**, *84*, 3013.
56. Peumans, P.; Forrest, S. R. *Appl. Phys. Lett.* **2001**, *79*, 126.
57. Hoth, C. N.; Schilinsky, P.; Choulis, S. A.; Brabec, C. J. *Nano Lett.* **2008**, *8*, 2806.
58. Padinger, F.; Rittberger, R. S.; Sariciftci, N. S. *Adv. Funct. Mater.* **2003**, *13*, 85.
59. Inakazu, F.; Noma, Y.; Ogomi, Y.; Hayase, S. *Appl. Phys. Lett.* **2008**, *93*, 093304.
60. Saikia, D.; Han, C. C.; Chen-Yang, Y. W. *J. Power Sources* **2008**, *185*, 570.
61. Kroon, J. M.; Bakker, N. J.; Smit, H. J. P.; Liska, P.; Thampi, K. R.; Wang, P.; Zakeeruddin, S. M.; Grätzel, M.; Hinsch, A.; Hore, S.; Würfel, U.; Sastrawan, R.; Durrant, J. R.; Palomares, E.; Petterson, H.; Gruszecki, T.; Walter, J.; Skupien, K.; Tulloch, G. E. *Prog. Photovoltaics Res. Appl.* **2007**, *15*, 1.
62. Beek, W. J. E.; Wienk, M. M.; Janssen, R. A. J. *Adv. Mater.* **2004**, *16*, 1009.
63. Sun, B.; Snaith, H. J.; Dhoot, A. S.; Westenhoff, S.; Greenham, N. C. *J. Appl. Phys.* **2005**, *97*, 014914.
64. Marcus, R. A. *Rev. Mod. Phys.* **1993**, *65*, 599.
65. Bolton, J. R.; Archer, M. D. *Adv. Chem. Ser.* **1991**, *228*, 7.
66. El-Khouly, M. E.; Ito, O.; Smith, P. M.; D'Souza, F. J. *Photochem. Photobiol. C* **2004**, *5*, 79.
67. Gouloumis, A.; de la Escosura, A.; Vázquez, P.; Torres, T.; Kahnt, A.; Guldi, D. M.; Neugebauer, H.; Winder, C.; Drees, M.; Sariciftci, N. S. *Org. Lett.* **2006**, *8*, 5187.

68. Lo, P.-C.; Leng, X.; Ng, D. K. P. *Coord. Chem. Rev.* **2007**, *251*, 2334.
69. Owens, J. W.; Smith, R.; Robinson, R.; Robins, M. *Inorg. Chim. Acta* **1998**, *279*, 226.
70. Ermilov, E. A.; Tannert, S.; Werncke, T.; Choi, M. T. M.; Ng, D. K. P.; Röder, B. *Chem. Phys.* **2006**, *328*, 428.
71. Ito, F.; Ishibashi, Y.; Khan, S. R.; Miyasaka, H.; Kameyama, K.; Morisue, M.; Satake, A.; Ogawa, K.; Kobuke, Y. *J. Phys. Chem. A* **2006**, *110*, 12734.
72. Konishi, T.; Ikeda, A.; Shinkai, S. *Tetrahedron* **2005**, *61*, 4881.
73. Vehmanen, V.; Tkachenko, N. V.; Imahori, H.; Fukuzumi, S.; Lemmetyinen, H. *Spectrochim. Acta A* **2001**, *57*, 2229.
74. Muströph, H.; Stollenwerk, M.; Bressau, V. *Angew. Chem. Int. Ed.* **2006**, *45*, 2016.
75. Meunier, B.; Sorokin, A. *Acc. Chem. Res.* **1997**, *30*, 470.
76. Ali, H.; van Lier, J. E. *Chem. Rev.* **1999**, *99*, 2379.
77. Kameyama, K.; Satake, A.; Kobuke, Y. *Tetrahedron Lett.* **2004**, *45*, 7617.
78. Prinzbach, H.; Weiler, A.; Landenberger, P.; Wahl, F.; Wörth, J.; Scott, L. T.; Belmont, M.; Olevano, D.; v. Issendorff, B. *Nature* **2000**, *407*, 60.
79. Krätschmer, W.; Lamb, L. D.; Fostiropoulos, K.; Huffman, D. R. *Nature* **1990**, *347*, 354.
80. Bühl, M.; Hirsch, A. *Chem. Rev.* **2001**, *101*, 1153.
81. Kroto, H. W.; Allaf, A. W.; Balm, S. P. *Chem. Rev.* **1991**, *91*, 1213.
82. Kroto, H. W.; Heath, J. R.; O'Brien, S. C.; Curl, R. F.; Smalley, R. E. *Nature* **1985**, *318*, 162.
83. Xie, Q.; Pérez-Cordero, E.; Echegoyen, L. *J. Am. Chem. Soc.* **1992**, *114*, 3978.
84. Araki, Y.; Chitta, R.; Sandanayaka, A. S. D.; Langenwalter, K.; Gadde, S.; Zandler, M. E.; Ito, O.; D'Souza, F. *J. Phys. Chem. C* **2008**, *112*, 2222.
85. Kozaki, M.; Akita, K.; Suzuki, S.; Okada, K. *Org. Lett.* **2007**, *9*, 3315.
86. Lapiński, A.; Graja, A.; Olejniczak, I.; Bogucki, A.; Imahori, H. *Chem. Phys.* **2004**, *305*, 277.
87. Possamai, G.; Camaioni, N.; Ridolfi, G.; Franco, L.; Ruzzi, M.; Menna, E.; Casalbore-Miceli, G.; Fichera, A. M.; Scorrano, G.; Corvaja, C.; Maggini, M. *Synth. Met.* **2003**, *139*, 585.
88. Martín, N.; Sánchez, L.; Illescas, B.; Pérez, I. *Chem. Rev.* **1998**, *98*, 2527.
89. Boyd, P. D. W.; Reed, C. A. *Acc. Chem. Res.* **2005**, *38*, 235.

90. Chukharev, V.; Tkachenko, N. V.; Efimov, A.; Lemmetyinen, H. *Chem. Phys. Lett.* **2005**, *411*, 501.
91. Hasobe, T.; Kamat, P. V.; Absalom, M. A.; Kashiwagi, Y.; Sly, J.; Crossley, M. J.; Hosomizu, K.; Imahori, H.; Fukuzumi, S. *J. Phys. Chem. B* **2004**, *108*, 12865.
92. Imahori, H. *Org. Biomol. Chem.* **2004**, *2*, 1425.
93. Guldi, D. M. *Pure Appl. Chem.* **2003**, *75*, 1069.
94. Kesti, T. J.; Tkachenko, N. V.; Yamada, H.; Imahori, H.; Fukuzumi, S.; Lemmetyinen, H. *Photochem. Photobiol. Sci.* **2003**, *2*, 251.
95. Kesti, T.; Tkachenko, N.; Vehmanen, V.; Yamada, H.; Imahori, H.; Fukuzumi, S.; Lemmetyinen, H. *J. Am. Chem. Soc.* **2002**, *124*, 8067.
96. Guldi, D. M.; Luo, C.; Da Ros, T.; Prato, M.; Dietel, E.; Hirsch, A. *Chem. Commun.* **2000**, 375.
97. Imahori, H.; Sakata, Y. *Eur. J. Org. Chem.* **1999**, 2445.
98. Schuster, D. I.; Li, K.; Guldi, D. M.; Palkar, A.; Echegoyen, L.; Stanisky, C.; Cross, R. J.; Niemi, M.; Tkachenko, N. V.; Lemmetyinen, H. *J. Am. Chem. Soc.* **2007**, *129*, 15973.
99. Luo, C.; Guldi, D. M.; Imahori, H.; Tamaki, K.; Sakata, Y. *J. Am. Chem. Soc.* **2000**, *122*, 6535.
100. Wiberg, J.; Guo, L.; Pettersson, K.; Nilsson, D.; Ljungdahl, T.; Mårtensson, J.; Albinsson, B. *J. Am. Chem. Soc.* **2007**, *129*, 155.
101. Di Valentin, M.; Bisol, A.; Agostini, G.; Liddell, P. A.; Kodis, G.; Moore, A. L.; Moore, T. A.; Gust, D.; Carbonera, D. *J. Phys. Chem. B* **2005**, *109*, 14401.
102. D'Souza, F.; Smith, P. M.; Gadde, S.; McCarty, A. L.; Kullman, M. J.; Zandler, M. E.; Ito, M.; Araki, Y.; Ito, O. *J. Phys. Chem. B* **2004**, *108*, 11333.
103. Imahori, H.; Yamada, H.; Nishimura, Y.; Yamazaki, I.; Sakata, Y. *J. Phys. Chem. B* **2000**, *104*, 2099.
104. Chiang, C. K.; Fincher, C. R. Jr.; Park, Y. W.; Heeger, A. J.; Shirakawa, H.; Louis, E. J.; Gau, S. C.; MacDiarmid, A. G. *Phys. Rev. Lett.* **1977**, *39*, 1098.
105. Shirakawa, H.; Louis, E. J.; MacDiarmid, A. G.; Chiang, C. K.; Heeger, A. J. *J. C. S. Chem. Comm.* **1977**, 578.
106. Facchetti, A. *Mater. Today* **2007**, *10*, 28.
107. Chabynyc, M. L.; Loo, Y-L. *J. Macromol. Sci., Polym. Rev.* **2006**, *46*, 1.
108. Moliton, A.; Hiorns, R. C. *Polym. Int.* **2004**, *53*, 1397.
109. Heeger, A. J. *J. Phys. Chem. B* **2001**, *105*, 8475.

110. de Gans, B.-J.; Duineveld, P. C.; Schubert, U. S. *Adv. Mater.* **2004**, *16*, 203.
111. Sheats, J. R. *J. Mater. Res.* **2004**, *19*, 1974.
112. Loo, Y.-L.; Someya, T.; Baldwin, K. W.; Bao, Z.; Ho, P.; Dodabalapur, A.; Katz, H. E.; Rogers, J. A. *Proc. Nat. Acad. Sci.* **2002**, *99*, 10252.
113. Ma, L.; Liu, J.; Pyo, S.; Yang, Y. *Appl. Phys. Lett.* **2002**, *80*, 362.
114. Friend, R. H.; Gymer, R. W.; Holmes, A. B.; Burroughes, J. H.; Marks, R. N.; Taliani, C.; Bradley, D. D. C.; Dos Santos, D. A.; Brédas, J. L.; Lögdlund, M.; Salaneck, W. R. *Nature* **1999**, *397*, 121.
115. Schilinsky, P.; Waldauf, C.; Hauch, J.; Brabec, C. J. *Thin Solid Films* **2004**, *451–452*, 105.
116. Koetse, M. M.; Sweelssen, J.; Hoekerd, K. T.; Schoo, H. F. M.; Veenstra, S. C.; Kroon, J. M.; Yang, X.; Loos, J. *Appl. Phys. Lett.* **2006**, *88*, 083504.
117. Chandrasekhar, P. *Conducting Polymers, Fundamentals and Applications*; Kluwer Academic Publishers: Dordrecht, **1999**.
118. Roncali, J. *Chem. Rev.* **1992**, *92*, 711.
119. Morita, S.; Zakhidov, A. A.; Yoshino, K. *Solid State Commun.* **1992**, *82*, 249.
120. Sariciftci, N. S.; Smilowitz, L.; Heeger, A. J.; Wudl, F. *Science* **1992**, *258*, 1474.
121. Colladet, K.; Fourier, S.; Cleij, T. J.; Lutsen, L.; Gelan, J.; Vanderzande, D.; Nguyen, L. H.; Neugebauer, H.; Sariciftci, N. S.; Aguirre, A.; Janssen, G.; Goovaerts, E. *Macromolecules* **2007**, *40*, 65.
122. Jespersen, K. G.; Zhang, F.; Gadisa, A.; Sundström, V.; Yartsev, A.; Inganäs, O. *Org. Electron.* **2006**, *7*, 235.
123. Yoo, S.; Potscavage, W. J.; Domercq, B.; Kim, J.; Holt, J.; Kippelen, B. *Appl. Phys. Lett.* **2006**, *89*, 233516.
124. Al-Ibrahim, M.; Sensfuss, S.; Uziel, J.; Ecke, G.; Ambacher, O. *Sol. Energy Mater. Sol. Cells* **2005**, *85*, 277.
125. Ma, W.; Yang, C.; Gong, X.; Lee, K.; Heeger, A. J. *Adv. Funct. Mater.* **2005**, *15*, 1617.
126. Ago, H.; Petritsch, K.; Shaffer, M. S. P.; Windle, A. H.; Friend, R. H. *Adv. Mater.* **1999**, *11*, 1281.
127. Onoda, M.; Tada, K.; Zakhidov, A. A.; Yoshino, K. *Thin Solid Films* **1998**, *331*, 76.
128. Kraabel, B.; Hummelen, J. C.; Vacar, D.; Moses, D.; Sariciftci, N. S.; Heeger, A. J.; Wudl, F. *J. Chem. Phys.* **1996**, *104*, 4267.

129. Peterson, I. R. *J. Phys. D: Appl. Phys.* **1990**, *23*, 379.
130. Roberts, G. *Langmuir–Blodgett Films*; Plenum Press: New York, **1990**.
131. Swalen, J. D.; Allara, D. L.; Andrade, J. D.; Chandross, E. A.; Garoff, S., Israelachvili, J.; McCarthy, T. J.; Murray, R.; Pease, R. F.; Rabolt, J. F.; Wynne, K. J.; Yu, H. *Langmuir* **1987**, *3*, 932.
132. Blodgett, K. B. *J. Am. Chem. Soc.* **1935**, *57*, 1007.
133. Mann, B.; Kuhn, H. *J. Appl. Phys.* **1971**, *42*, 4398.
134. Charitat, T.; Bellet-Amalric, E.; Fragneto, G.; Graner, F. *Eur. Phys. J. B* **1999**, *8*, 583.
135. Giebeler, C.; Marks, R. N.; Bleyer, A.; Bradley, D. D. C.; Schrader, S. *Opt. Mater.* **1998**, *9*, 99.
136. Lehtivuori, H.; Lemmetyinen, H.; Tkachenko, N. V. *J. Am. Chem. Soc.* **2006**, *128*, 16036.
137. Efimov, A.; Vainiotalo, P.; Tkachenko, N. V.; Lemmetyinen, H. *J. Porphyrins Phthalocyanines* **2003**, *7*, 593.
138. Isosoppi, M.; Tkachenko, N. V.; Efimov, A.; Vahasalo, H.; Jukola, J.; Vainotalo, P.; Lemmetyinen, H. *Chem. Phys. Lett.* **2006**, *430*, 36.
139. Flueraru, C.; Schrader, S.; Zauls, V.; Motschmann, H.; Stiller, B.; Kiebooms, R. *Synth. Met.* **2000**, *111–112*, 603.
140. Dautel, O. J.; Wantz, G.; Almairac, R.; Flot, D.; Hirsch, L.; Lere-Porte, J-P.; Parneix, J-P.; Serein-Spirau, F.; Vignau, L.; Moreau, J. J. E. *J. Am. Chem. Soc.* **2006**, *128*, 4892.
141. Han, K.; Ma, S.; Lu, X. *Opt. Commun.* **1995**, *118*, 74.
142. Tkachenko, N. V.; Vuorimaa, E.; Kesti, T.; Alekseev, A. S.; Tauber, A. Y.; Hynninen, P. H.; Lemmetyinen, H. *J. Phys. Chem. B* **2000**, *104*, 6371.
143. Tkachenko, N. V.; Tauber, A. Y.; Hynninen, P. H.; Sharonov, A. Y.; Lemmetyinen, H. *J. Phys. Chem. A* **1999**, *103*, 3657.
144. Ikonen, M.; Sharonov, A.; Tkachenko, N. V.; Lemmetyinen, H. *Adv. Mater. Opt. Electron.* **1993**, *2*, 115.
145. Tkachenko, N. *Optical Spectroscopy, Methods and Instrumentations*; Elsevier: Boston, **2006**.
146. Vehmanen, V.; Tkachenko, N. V.; Efimov, A.; Damlin, P.; Ivaska, A.; Lemmetyinen, H. *J. Phys. Chem. A* **2002**, *106*, 8029.

147. Alekseev, A. S.; Tkachenko, N. V.; Tauber, A. Y.; Hynninen, P. H.; Österbacka, R.; Stubb, H.; Lemmetyinen, H. *Chem. Phys.* **2002**, *275*, 243.
148. Manoj, A. G.; Narayan, K. S. *Opt. Mater.* **2002**, *21*, 417.
149. Yun, J-J.; Jung, H-S.; Kim, S-H.; Han, E-M.; Vaithianathan, V.; Jenekhe, S. A. *Appl. Phys. Lett.* **2005**, *87*, 123102.
150. Imahori, H.; Norieda, H.; Yamada, H.; Nishimura, Y.; Yamazaki, I.; Sakata, Y.; Fukuzumi, S. *J. Am. Chem. Soc.* **2001**, *123*, 100.
151. Fujitsuka, M.; Ito, O.; Yamashiro, T.; Aso, Y.; Otsubo, T. *J. Phys. Chem. A* **2000**, *104*, 4876.
152. Wintgens, V.; Valat, P.; Garnier, F. *J. Phys. Chem.* **1994**, *98*, 228.
153. Fujitsuka, M.; Masuhara, A.; Kasai, H.; Oikawa, H.; Nakanishi, H.; Ito, O.; Yamashiro, T.; Aso, Y.; Otsubo, T. *J. Phys. Chem. B* **2001**, *105*, 9930.
154. Nogueira, A. F.; Montanari, I.; Nelson, J.; Durrant, J. R.; Winder, C.; Sariciftci, N. S.; Brabec, C. *J. Phys. Chem. B* **2003**, *107*, 1567.
155. Offermans, T.; Meskers, S. C. J.; Janssen, R. A. J. *J. Chem. Phys.* **2003**, *119*, 10924.
156. Luo, J.; Peng, L-M.; Xue, Z. Q.; Wu, J. L. *J. Chem. Phys.* **2004**, *120*, 7998.
157. Toniolo, R.; Hümmelgen, I. A. *Macromol. Mater. Eng.* **2004**, *289*, 311.
158. Ghosh, A. P.; Gerenser, L. J.; Jarman, C. M.; Fornalick, J. E. *Appl. Phys. Lett.* **2005**, *86*, 223503.
159. Natali, D.; Sampietro, M. *Nucl. Instrum. Methods Phys. Res., Sect. A* **2003**, *512*, 419.
160. Frycek, R.; Jelínek, M.; Kocourek, T.; Fitl, P.; Vrnata, M.; Myslik, V.; Vrbova, M. *Thin Solid Films* **2006**, *495*, 308.
161. Logothetidis, S. *Mater. Sci. Eng., B* **2008**, *152*, 96.